The molar volume of FeO–MgO–Fe_2O_3–Cr_2O_3–Al_2O_3–TiO_2 spinels

Emily A. Hamecher, Paula M. Antoshechkina, Mark S. Ghiorso & Paul D. Asimow

Contributions to Mineralogy and Petrology

ISSN 0010-7999

Contrib Mineral Petrol
DOI 10.1007/s00410-012-0790-0

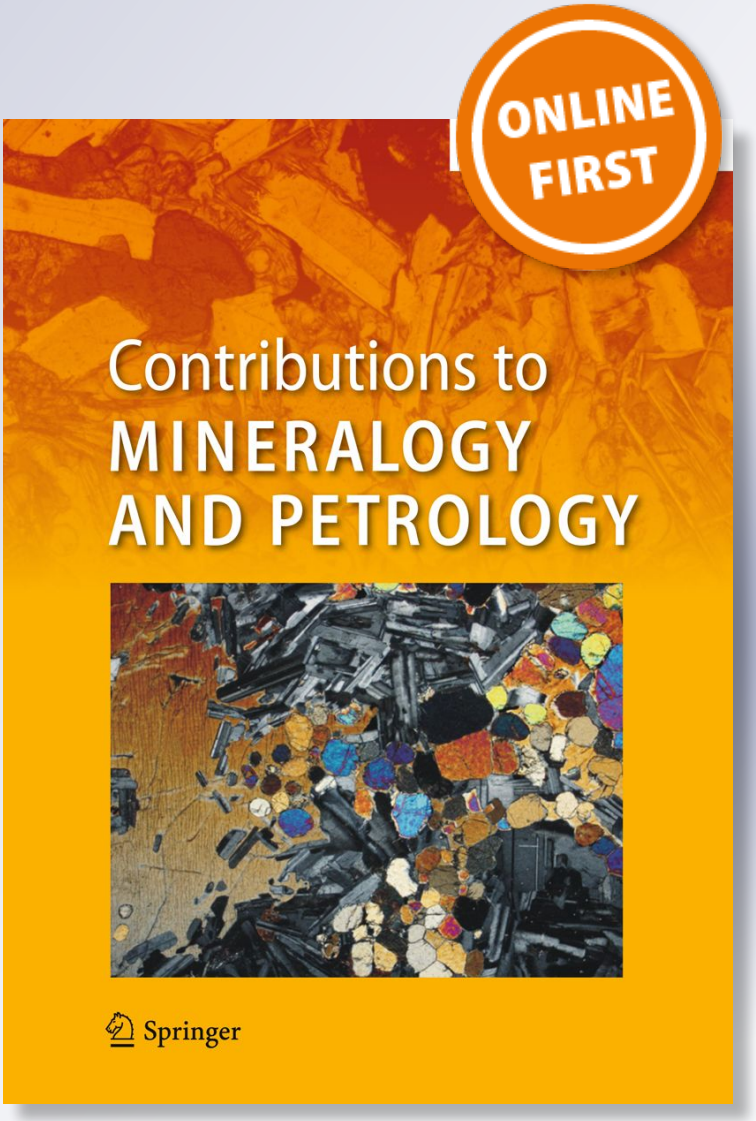

Springer

Contrib Mineral Petrol
DOI 10.1007/s00410-012-0790-0

ORIGINAL PAPER

The molar volume of $FeO–MgO–Fe_2O_3–Cr_2O_3–Al_2O_3–TiO_2$ spinels

Emily A. Hamecher · Paula M. Antoshechkina · Mark S. Ghiorso · Paul D. Asimow

Received: 28 September 2011 / Accepted: 31 July 2012

Abstract We define and calibrate a new model of molar volume as a function of pressure, temperature, ordering state, and composition for spinels in the supersystem (Mg, Fe^{2+})(Al, Cr, Fe^{3+})$_2O_4$ − (Mg, Fe^{2+})$_2TiO_4$. We use 832 X-ray and neutron diffraction measurements performed on spinels at ambient and in situ high-P, T conditions to calibrate end-member equations of state and an excess volume model for this system. The effect on molar volume of cation ordering over the octahedral and tetrahedral sites is captured with linear dependence on Mg^{2+}, Al^{3+}, and Fe^{3+} site occupancy terms. We allow standard-state volumes and coefficients of thermal expansion of the end members to vary within their uncertainties during extraction of the mixing properties, in order to achieve the best fit. Published equations of state of the various spinel end members are analyzed to obtain optimal values of the bulk modulus and its pressure derivative, for each explicit end member. For any spinel composition in the supersystem, the model molar volume is obtained by adding excess volume and cation order-dependent terms to a linear combination of the five end-member volumes, estimated at pressure and temperature using the high-T Vinet equation of state. The preferred model has a total of 9 excess volume and order-dependent parameters and fits nearly all experiments to within 0.02 J/bar/mol, or better than 0.5 % in volume. The model is compared to the current MELTS spinel model with a demonstration of the impact of the model difference on the estimated spinel-garnet lherzolite transition pressure.

Keywords Spinel · Molar volume · Thermodynamic modeling · MELTS

Communicated by J. Blundy.

Electronic supplementary material The online version of this article (doi:10.1007/s00410-012-0790-0) contains supplementary material, which is available to authorized users.

E. A. Hamecher (✉) · P. M. Antoshechkina · P. D. Asimow
Division of Geological and Planetary Sciences,
California Institute of Technology, Pasadena, CA 91125, USA
e-mail: hamecher@gps.caltech.edu

M. S. Ghiorso
OFM Research, 7336 24th Ave NE, Seattle, WA 98115, USA

Introduction

Spinel-group minerals are commonly found in igneous and metamorphic rocks in the Earth's crust and upper mantle and are frequently used as petrogenetic indicators (Buddington and Lindsley 1964; Sack 1982; Dick and Bullen 1984; Ghiorso and Sack 1991; Ghiorso and Evans 2008). Spinel is a significant reference phase for high-pressure thermodynamic solution models of melts and of other solid phases, because it contains several key components of upper mantle assemblages at appreciable concentrations and because high-quality activity-composition models for spinels have been constructed (Sack 1982; Nell and Wood 1989; Sack and Ghiorso 1991a, b; Kessel et al. 2003). Beyond their petrologic significance, natural and synthetic spinel-group phases have numerous applications in the material sciences (e.g., Taberna et al. 2006; Yang et al. 2007).

The prevalence of spinels can be partly explained by the variety of cations of different valence that can be accommodated within the structure. While the spinel structure is quite simple, its solid solution behavior is complex. Cubic spinels (space group $Fd3m$) have the stoichiometry AB_2O_4, where A and B are cations with, most often, 2+ and 3+ charge, respectively, although substitution toward end members where A is 4+ and B is 2+ can occur. Additional

Published online: 24 August 2012

complexity arises due to the existence of two distinct cation coordination environments and the ability of a wide array of cations to distribute themselves over the octahedral and tetrahedral crystallographic sites. "Normal" spinels are defined as having the *A* ion in the tetrahedral site and both *B* ions in the two identical octahedral sites. Perfectly "inverse" spinels have one *B* ion per formula unit occupying the tetrahedral site, with one *A* and one *B* ion residing in the octahedral sites. For many choices of *A* and *B*, spinel solid solutions can adopt ordering states at any point along this continuum. A number of models have described the extent of such ordering in spinels (Callen et al. 1956; O'Neill and Navrotsky 1983, 1984; Sack and Ghiorso 1991a) in terms of the energetics of the cation-ordering reactions.

Molar volume is an important thermodynamic quantity at high pressures, both when using spinels to infer petrogenetic information from high-pressure rocks and particularly when using spinels from high-pressure experiments to define chemical potentials in coexisting phases. Because pressures of interest in spinel-bearing experiments range up to at least 3 GPa (3×10^4 bar), differences in volume of only 0.03 J/bar/mol (i.e., 0.3 cm^3/mol, or $\leq$1 % of typical spinel molar volumes) yield differences of 1 kJ/mol in chemical potentials, which is often the accuracy level sought in calibrations of solid- and liquid-solution models. A model of spinel volumes with the necessary accuracy needs to account not only for equations of state of pure end members and considerable deviation from ideal mixing of compositions but also for significant effects of ordering state on the volume (O'Neill and Navrotsky 1983; Hazen and Navrotsky 1996). Differences in ionic size, charge, and/or coordination environment can contribute to non-ideal behavior (O'Neill and Navrotsky 1984). Pressure, in addition to temperature and composition, can strongly affect cation-ordering state, which in turn affects physical properties, including the elastic moduli (Hazen and Navrotsky 1996). The complexities due to cation ordering over distinct crystallographic sites, along with the wide range of stable compositions of spinels, create difficulties in modeling their thermodynamic behavior, including molar volume (Sack and Ghiorso 1991a). Generally, studies are restricted to subsystems of spinels, for example, along a solid-solution binary. While limiting the system of interest usually allows one to recover the data used in calibration, discrepancies exist between various end-member models, that is, a particular spinel end member may be assigned different model volumes in fits to adjacent subsystems. Hence, currently available models are inadequate for modeling of volumes over the full compositional range of spinels formed in the Earth's upper mantle. It is necessary to devise a comprehensive model applicable to the entire chemical system of the upper mantle.

In this work, we present a model of molar volumes of stoichiometric spinels containing the oxide components FeO-MgO-Fe_2O_3-Cr_2O_3-Al_2O_3-TiO_2; the cations in this system account for at least 98 % of the compositional range of natural spinels (Sack 1982). Our chosen set of independent compositional model end members is as follows: spinel sensu stricto ($MgAl_2O_4$), hercynite ($FeAl_2O_4$), magnetite (Fe_3O_4), chromite ($FeCr_2O_4$), and ulvöspinel (Fe_2TiO_4). Dependent end members in this system—magnesiochromite ($MgCr_2O_4$), magnesioferrite ($MgFe_2O_4$), and qandilite (Mg_2TiO_4)—are formed from linear combinations of the independent end members. As written, these are *compositional* end members only, and the order in which the cations are written should not be taken to imply an ordering state over tetrahedral and octahedral sites. Within the MELTS software, end-member thermodynamic quantities are calculated for the standard-state structural arrangement, and mixing properties are referenced to the end-member values. For calibration of the volume, we are therefore obliged to use end members with the ordering states adopted by Sack and Ghiorso (1991a, b), that is, normally ordered $FeCr_2O_4$ and Fe_2TiO_4, almost perfectly normal $MgAl_2O_4$ and $FeAl_2O_4$, and near-perfect inversely ordered Fe_3O_4. Note that this constraint did not apply to Sack and Ghiorso's formulation of the activity-composition models, as the adopted end-member heat capacity functions (taken from the internally consistent database of Berman 1988) were independent of ordering state. In fact, the Sack and Ghiorso (1991a, b) model was calibrated using perfectly inverse ordered components; normally ordered and standard-state values for the compositional components were inferred from the fitted parameters.

Our primary motivation in this work is to develop a comprehensive spinel molar volume model for use in calibration of activity-composition models of garnet and pyroxene solid solutions. The thermodynamic models, along with a new silicate liquid equation of state (Ghiorso 2004a, b, c; Ghiorso and Kress 2004), will be incorporated into the next generation MELTS (Ghiorso and Sack 1995; Ghiorso et al. 2002; Asimow et al. 2004) model, xMELTS (Ghiorso et al. 2007). The new solid solution models will include some minor components, including Ti^{4+} and Cr^{3+}. Because most constraints on the activity of garnets and pyroxenes at high-*P* are derived from experiments with coexisting spinels, we must be confident in the ability of our spinel model to realistically reproduce thermodynamic behavior over the entire applicable range of compositions. Additionally, producing a spinel molar volume model calibrated with recent in situ high-(*P, T*) X-ray and neutron diffraction data is crucial to our ability to accurately model the spinel-garnet transition in Earth's upper mantle. For example, we recently calibrated Cr–Al exchange equilibria for garnet and spinel (Hamecher et al. 2009). When this

new calibration is used with the current MELTS model, a region of garnet–spinel coexistence in lherzolites is predicted with width in pressure comparable to experimental constraints. The transition occurs, however, at the unexpectedly low pressure of $\sim$1.7 GPa, though this is not entirely due to the introduction of Cr to the system, as discussed below. The improved model of spinel molar volume presented here will enable coupled recalibration of the garnet and pyroxene models to match both the absolute pressure and width of this key transition in mantle lithology.

In this paper, we first discuss previous models of spinel molar volume, with attention to the ranges of composition they cover and inconsistencies among the models. We then present the X-ray and neutron diffraction and ultrasonic data used in our calibration, and the formulation of our model in terms of the components and ordering variables of the spinel solid solution model of Sack and Ghiorso (1991a, b). The calibration strategy we used to estimate the parameters of the model and assess goodness-of-fit to the data is outlined. Finally, we compare the final model to models from the literature and present an estimate of the magnitude of the impact of the new model on MELTS calculations and other high-pressure thermodynamic inferences.

Previous models

Several models for the molar volume of spinel-group minerals have been proposed. However, most of these models are restricted to binary subsystems. Furthermore, there are discrepancies between models with corresponding end members. In this section, we present examples of previous models of spinel molar volume.

The current molar volume model for spinels in MELTS and pMELTS covers the same compositional range as our proposed model. There is no mention of volume in Sack and Ghiorso (1991a) or Sack and Ghiorso (1991b) and, indeed, initially the entire system was assumed to have zero volume of mixing. However, before being put to use for calculation or calibration of other phases, the model was modified to include asymmetric excess volume of mixing terms along the Fe_3O_4–Fe_2TiO_4 join (Ghiorso 1990; Ghiorso and Sack 1991): an excess model of the form $-0.1250X^2_{Fe_3O_4}X_{Fe_2TiO_4} + 0.1018X_{Fe_3O_4}X^2_{Fe_2TiO_4}$ J/bar/mol was fitted to the molar volume data of Lindsley (1965). This excess term was used in the calibration of subsequent models including the pyroxene family (Sack and Ghiorso 1994b), the MELTS liquid model (Ghiorso and Sack 1995), and the pMELTS liquid model (Ghiorso et al. 2002) and is present in all currently supported versions of the MELTS code. As part of the provisional xMELTS liquid model calibration, the spinel volume model was extended to higher pressures by fitting the formula for the high-T Vinet equation of state (see Eq. 6 below) for $MgAl_2O_4$ and Fe_3O_4 to the Berman (1988) polynomial equation of state (see Ghiorso 2004b). Since standard-state volume data for other spinel components are not given in Berman (1988), P- and T-coefficients for $MgAl_2O_4$ or Fe_3O_4 were assigned to the remaining end members. There is now an opportunity to simultaneously optimize both standard state and mixing terms in order to form an internally consistent general spinel system volume model for use in future calibration and calculation efforts. Our recalibration includes refinement of the asymmetric terms along the Fe_3O_4–Fe_2TiO_4 join alongside consideration of all other possible binary excess terms in the composition space.

Oka et al. (1984) fit their molar volume data along the $MgAl_2O_4 - MgCr_2O_4$ binary to an asymmetric regular solution model $W_{AlAlCr}(1 - X_{Cr})^2X_{Cr} + W_{AlCrCr}(1 - X_{Cr})X^2_{Cr}$ (where X_{Cr} is mole fraction $MgCr_2O_4$ for this binary). For their best-characterized data, synthesized at 1,250 °C, they obtained excess volume parameters $W_{AlAlCr} = 0.0524(91)$ and $W_{AlCrCr} = 0.0040(92)$ J/bar/mol. On the other hand, average parameters for fits to three different sets of synthesis temperatures are $W_{AlAlCr} = 0.0504$ and $W_{AlCrCr} = 0.0182$ J/bar/mol (uncertainties not stated). Both versions of the model show positive deviation from ideality along the entire binary.

Doroshev et al. (1997) also investigated the molar volume of the $MgAl_2O_4 - MgCr_2O_4$ subsystem. Phase equilibria experiments containing Cr-rich garnets were performed, and the multiphase products were analyzed by electron microprobe and X-ray diffraction. Doroshev et al. also adopted an asymmetric regular solution excess volume model, with the largest deviation from ideality in the Al-rich part of the join. Contrary to the previous study, however, Doroshev et al. found negative deviation from ideality in the Cr-rich region: the excess volume parameters are $W_{AlAlCr} = 0.0722(90)$ and $W_{AlCrCr} = -0.0483(75)$ J/bar/mol. The authors attribute the difference between the models to a more thorough characterization of the Cr-rich samples.

Brey et al. (1999) performed similar experiments to Doroshev et al. (1997), but in the larger system FeO-MgO-Al_2O_3-SiO_2-Cr_2O_3. The explicit spinel end members in the Brey et al. model are $MgAl_2O_4$, $FeCr_2O_4$, and $MgCr_2O_4$. After considering a possible nonzero volume of reaction for the reciprocal (cross-site) reaction, Brey et al. discard this term. They retain an excess mixing volume due to exchange of Mg^{2+} and Fe^{2+} cations, fit by a symmetric model with the parameter $W_{FeMg} = -0.020(7)$ J/bar/mol. Also, like Doroshev et al., Brey et al. use an asymmetric excess volume model for the Cr^{3+}-Al^{3+} exchange with parameters (recast into common form with above models) $W_{AlCrCr} = 0.034(18)$ and $W_{AlCrCr} = -0.014(12)$ J/bar/

mol. This fit retains a negative deviation from ideality for Cr-rich compositions, but this result is only marginally significant, and does not fit the pure Fe-free data of Doroshev et al. and Oka et al. (1984) especially well.

Mattioli et al. (1987) derived a model of the volume of the ternary spinel system $MgAl_2O_4$–Fe_3O_4–$\gamma Fe_{8/3}O_4$. The volumes of the Fe_3O_4–$\gamma Fe_{8/3}O_4$ and $MgAl_2O_4$–$\gamma Fe_{8/3}O_4$ edges of this ternary system are treated as ideal. The $MgAl_2O_4$–Fe_3O_4 join is modeled as an asymmetric regular solution model, of the same form discussed above, with excess volume parameters $W_{\text{mt-mt-sp}} = 0.075(17)$ and $W_{\text{mt-sp-sp}} = 0.18(5)$ J/bar/mol, where mt = Fe_3O_4 and sp = $MgAl_2O_4$. In our final model, we find that an asymmetric excess volume term along the $MgAl_2O_4$–Fe_3O_4 binary is not justified by the data at ambient pressure and thus treat this join as symmetric.

Three choices of solid solution model for spinel, each one based on the thermodynamic dataset of Holland and Powell (1998), are included in the modeling package THERMOCALC (e.g., Powell et al. 1998; currently hosted at http://www.metamorph.geo.uni-mainz.de/thermocalc/). None of the models incorporate any excess volume terms. The latest version of the thermodynamic database (Holland and Powell 2011) uses a modified equation of state that may be more easily extrapolated to very high pressures than the Murnaghan equation of state used in Holland and Powell (1998). Updated solid solution models have yet to be released. The Perple_X modeling package (e.g., Connolly 2009) offers the potential to adopt a wide variety of solid solution models, including several of those mentioned above (see http://www.perplex.ethz.ch/). All of the spinel models treat the $MgAl_2O_4$–$FeAl_2O_4$ join as ideal in volume. Only one of the available thermodynamic databases includes a chrome-bearing component for spinel (Klemme et al. 2009). The corresponding solution model for MgO-FeO-Al_2O_3-Cr_2O_3 spinels adopts the formulation of Oka et al. (1984) for asymmetric excess volume due to Al^{3+}-Cr^{3+} exchange.

Data sources

The American Mineralogist Crystal Structure Database (AMCSD) (Downs and Hall-Wallace 2003) provides a comprehensive collection of published X-ray and neutron diffraction refinements of cell volume and site occupancy; we fit the entire database of spinels with *Fd3m* space group symmetry in the system FeO-MgO-Fe_2O_3-Cr_2O_3-Al_2O_3-TiO_2 (Figs. 1, 2). The very oldest studies (Bragg 1915; Passerini 1930; Verwey and Heilmann 1947) and all other spinels in the database—e.g., tetragonal spinels, franklinites, trevorites, and maghemites—were excluded. In addition, we found these data sources for refined site occupancy data not in the AMCSD: Carbonin et al. (1996), Della Giusta et al. (1996), Princivalle et al. (1999), and Levy et al. (2004). Furthermore, a few sources are available that provide cell parameter based on powder XRD and

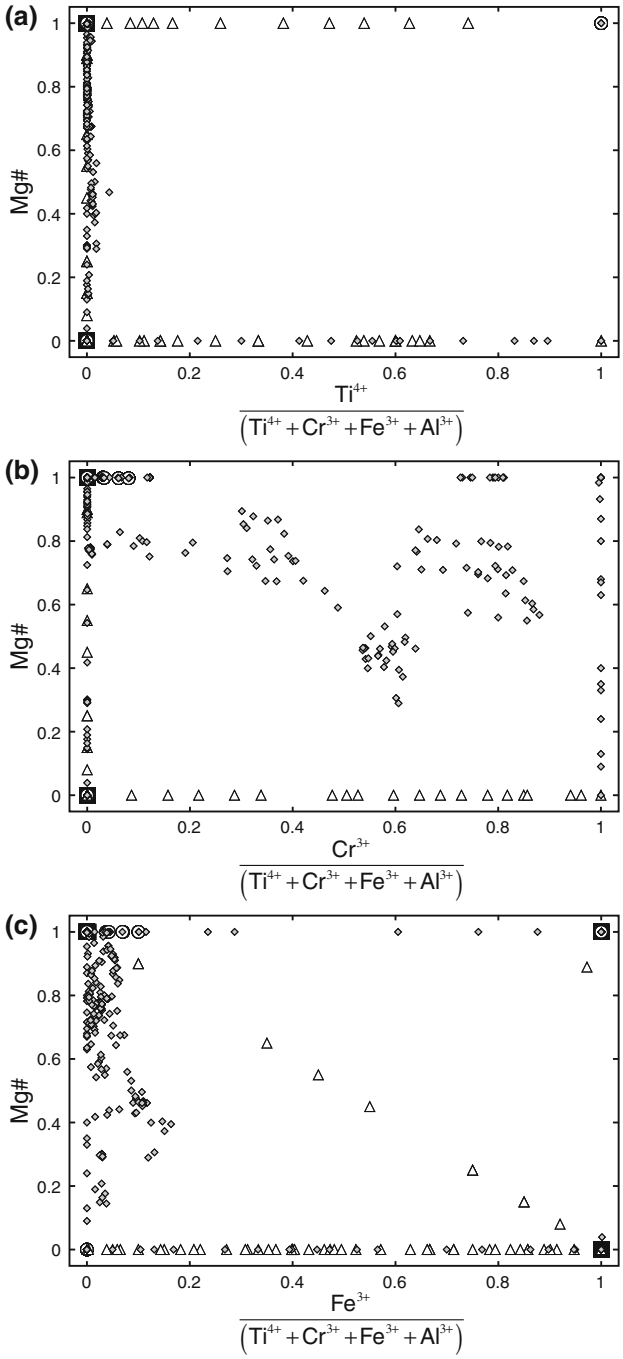

Fig. 1 Compositional coverage of the data used in model calibration. *Diamonds* are experiments measured at ambient conditions, *circles* are experiments measured at high-*T*, *squares* are data measured at high-*P*. *Triangles* are data not included in calibration due to lack of measured site occupancies and are used only for comparison with model results below. **a** Mg# (Mg/[Mg + Fe^{2+}]) versus $Ti^{4+}/(Ti^{4+} + Cr^{3+} + Fe^{3+} + Al^{3+})$; **b** Mg# versus $Cr^{3+}/(Ti^{4+} + Cr^{3+} + Fe^{3+} + Al^{3+})$; **c** Mg# versus $Fe^{3+}/(Ti^{4+} + Cr^{3+} + Fe^{3+} + Al^{3+})$

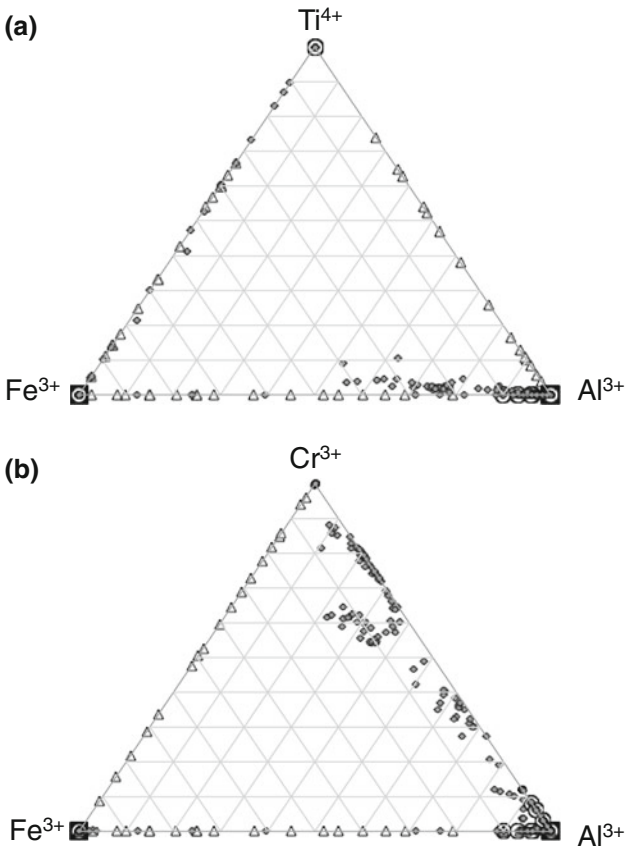

Fig. 2 Compositional coverage of the data used in model calibration. *Symbols* the same as in Fig. 1. **a** Ti^{4+} – Fe^{3+} – Al^{3+} ternary; **b** Cr^{3+} – Fe^{3+} – Al^{3+} ternary

electron microprobe analysis of an experimental charge (Doroshev et al. 1997; Brey et al. 1999; Girnis et al. 2003). We used these data by assuming the specimen was quenched from an equilibrium ordering state at experimental conditions and applying the ordering model built into MELTS (Sack and Ghiorso 1991a, b). This approximation introduces two potential sources of error: (a) the temperature recorded by the true ordering state may be lower than the experimental one and (b) there is an inherent uncertainty associated with the MELTS ordering model (e.g., a consequence of the simplistic spinel volume model in MELTS is that the predicted ordering state is independent of pressure). Both errors are probably systematic and the restricted compositional and *P–T* ranges mean that the data are likely to be affected to a similar degree. Hence, although the measurements were given slightly less weight during the regression than those with accompanying site occupancy data, their inclusion is reasonable and the model fit is not substantially affected by the absence of measured site occupancies.

Our final model is calibrated using a total of 832 experiments. The compositional and *P–T* coverage of the data is summarized in Table 1. All references for data used in model calibration are listed in Electronic Supplementary Material 1. Experimental conditions, observed cell parameters, and cation site occupancies are given in Electronic Supplementary Material 2. There are a number of compositional gaps in the volume calibration database. Some are due to immiscibility (Barnes and Roeder 2001; Pascal et al. 2011), and some correspond to spinels found in lunar samples too precious for analysis by XRD (Haggerty 1971). Still others are filled by studies of binary spinels for which site occupancies were not characterized (Golla-Schindler et al. 2005; Mattioli et al. 1987; Muan et al. 1972; Robbins et al. 1971; Wechsler et al. 1984; Woodland et al. 2009; Zhao et al. 1998). Unlike the experimental studies discussed above, none of these measurements could be incorporated into the calibration dataset. Either the equilibration temperature could not be estimated sufficiently accurately or the measured volume trend disagreed with a reliable data source for one or other pure phase end member, even when ordering state could not be a factor. Hence, inclusion of these studies would have had a detrimental effect on the calibrated standard-state volumes. Nevertheless, the data were useful for comparison and (once allowance was made for any discrepancies in the end-member volume contributions) provided a valuable independent test of the newly calibrated model.

We assume that all Ti^{4+} (Wechsler et al. 1984; Sack and Ghiorso 1991a; Bosi et al. 2009) and all Cr^{3+} (Dunitz and Orgel 1957; Sack and Ghiorso 1991b) cations occupy the octahedral site in spinels. This choice is supported by the calibration dataset: of the data considered, only one $MgCr_2O_4$ (Tabira and Withers 1999), one Fe_2TiO_4 (Stout and Bayliss 1980), and one Mg_2TiO_4 (O'Neill et al. 2003) are reported as having 2 % or more of Ti^{4+} or Cr^{3+} partitioned onto the tetrahedral site. Thus, we assigned any reported tetrahedral Ti^{4+} and Cr^{3+} to the octahedral site, moving Mg^{2+} as needed to compensate for site occupancy and charge. For example,

$$\begin{aligned} {}^{[4]}X_{Mg^{2+}} &= {}^{[4]}X'_{Mg^{2+}} + {}^{[4]}X'_{Cr^{3+}} \\ {}^{[6]}X_{Mg^{2+}} &= {}^{[6]}X'_{Mg^{2+}} - \frac{1}{2}{}^{[4]}X'_{Cr^{3+}} \\ {}^{[6]}X_{Cr^{3+}} &= {}^{[6]}X'_{Cr^{3+}} + \frac{1}{2}{}^{[4]}X'_{Cr^{3+}}, \end{aligned} \quad (1)$$

where left superscript [4] denotes the tetrahedral site, [6] denotes the octahedral site, and *X'* represents the proportion of the indicated cation before the adjustment is made. The same relationships hold for the substitution of Ti^{4+} by replacing Cr^{3+} with Ti^{4+} in Eq. 1. Elements not included in our system were projected onto major cations of similar size and charge: Mn^{2+} and Mn^{3+} were assigned to Fe^{2+} and Fe^{3+}, respectively; the divalent cations Zn^{2+}, Ni^{2+}, and Co^{2+} were distributed proportionally over Mg^{2+} and Fe^{2+}; V^{3+} was projected onto Fe^{3+}; and Si^{4+} was cast into Ti^{4+}.

Table 1 Summary table of data coverage in composition, P and T

Composition	Total experiments	Ambient-P, T	High-P	P range (GPa)	High-T	T range (°C)
End members						
$MgAl_2O_4$	151	48	21	0.6–29	82	132–1,600
$FeCr_2O_4$	1	1	0	–	0	–
Fe_2TiO_4	2	2	0	–	0	–
Fe_3O_4	55	9	46	0.02–11.11	0	–
$FeAl_2O_4$	40	23	0	–	17	200–1,150
$MgCr_2O_4$	6	6	0	–	0	–
$MgFe_2O_4$	69	24	28	0.11–34.39	17	100–1,200
Mg_2TiO_4	53	2	0	–	51	70–1,416
Binaries						
$MgAl_2O_4$–$FeAl_2O_4$	14	14	0	–	0	–
$FeAl_2O_4$–Fe_3O_4	1	1	0	–	0	–
$FeTi_2O_4$–Fe_3O_4	18	18	0	–	0	–
$MgAl_2O_4$–$MgFe_2O_4$	68	15	4	1–4	49	200–1,050
$MgAl_2O_4$–$MgCr_2O_4$	194	87	34	4.4–8.03	73	200–1,000
$FeCr_2O_4$-$MgCr_2O_4$	13	13	0	–	0	–
Fe_3O_4–$MgFe_2O_4$	1	1	0	–	0	–
Multi-component	146	146	0	–	0	–
Total	832	410	133		289	

To limit the data used to fit the model to those spinels that are applicable to terrestrial or lunar mafic and ultramafic rocks, we developed a set of exclusion criteria. All experiments that contained vacancies on either crystallographic site were excluded. Likewise, experiments that contained Ca^{2+} were not included in the calibration, because even very small amounts of octahedral Ca^{2+} produced systematic errors in the model. We established a 5 % site occupancy threshold for the other minor elements, that is, we rejected experiments that reported greater than 5 % occupancy in either site of Mn^{2+}, Mn^{3+}, Ni^{2+}, Zn^{2+}, Co^{2+}, V^{3+}, or Si^{4+}. We noted no evidence that Jahn–Teller distortion affects the volume at the level of Mn^{3+} substitution allowed (Ishii et al. 1972). In order that the projected composition of all calibrated spinels conform to the stoichiometry of the chosen model end members, within a reasonable tolerance, we filtered out any site occupancy data with reported site totals differing from unity by more than ±0.01 and any data with total cation charge greater than +8.03 or less than +7.97 per formula unit.

One drawback with the chosen dataset is the lack of reliable error estimates for the observed and modeled molar volumes, which makes it difficult to weight the calibration data in any meaningful way. Errors on lattice parameters are estimated when data are curated in the AMCSD and suggest that the measurement precision values reported in the original sources can be misleadingly small. Room temperature fluctuations have a negligible effect on the total error, naturally, but inter-laboratory differences can be significant for in situ experiments at high-P, T; several of the high-T and high-P measurements have no reported bounds. Uncertainties associated with site occupancy determinations are almost never quantified but must vary depending on the type of sample (synthetic or natural), composition (end-member, binary, etc.), and measurement procedure. O'Neill and Dollase (1994) compared the effect of different refinement procedures on the final site occupancy distributions and several authors (e.g., Mattioli et al. 1987; O'Neill et al. 1992) have studied the effect of stoichiometry, or lack thereof, on molar volume. Given that it was impossible to come up with an automated strategy for assigning error estimates, we instead weighted all data equally but paid more attention to end-member and binary compositions when deciding between conflicting data or identifying outliers. This approach was later modified slightly to use weighted nonlinear least squares, where all data were assigned the same nominal standard error except those requiring the MELTS ordering model (Doroshev et al. 1997; Brey et al. 1999; Girnis et al. 2003) which were given a doubled value. Reasons and details are given above and in the electronic appendix (Electronic Supplementary Material 3).

Model formulation

For fitting molar volume data to our model, the data must first be recast in a consistent manner into the representation of composition and ordering state we adopted. Most of the

data we use are given in the AMCSD in the form of cation mole fractions on the tetrahedral and octahedral sites. For this kind of data, we first transformed the molar cation proportions into the following set of linearly independent compositional variables:

$$X_{\mathrm{sp}} = {}^{[4]}X_{\mathrm{Mg}^{2+}} + 2^{[6]}X_{\mathrm{Mg}^{2+}} \tag{2a}$$

$$X_{\mathrm{ch}} = {}^{[6]}X_{\mathrm{Cr}^{3+}} \tag{2b}$$

$$X_{\mathrm{uv}} = 2^{[6]}X_{\mathrm{Ti}^{4+}} \tag{2c}$$

$$X_{\mathrm{mt}} = \frac{1}{2}\left({}^{[4]}X_{\mathrm{Fe}^{3+}} + 2^{[6]}X_{\mathrm{Fe}^{3+}}\right), \tag{2d}$$

plus the dependent closure variable

$$X_{\mathrm{hc}} = 1 - X_{\mathrm{sp}} - X_{\mathrm{ch}} - X_{\mathrm{uv}} - X_{\mathrm{mt}}, \tag{2e}$$

where $\mathrm{sp} = MgAl_2O_4$, $\mathrm{ch} = FeCr_2O_4$, $\mathrm{uv} = Fe_2TiO_4$, $\mathrm{mt} = Fe_3O_4$, and $\mathrm{hc} = FeAl_2O_4$. The cation-ordering variables are:

$$s_0 = {}^{[4]}X_{\mathrm{Mg}^{2+}} - 2^{[6]}X_{\mathrm{Mg}^{2+}} \tag{3a}$$

$$s_1 = \frac{1}{2}\left(2^{[6]}X_{\mathrm{Al}^{3+}} - {}^{[4]}X_{\mathrm{Al}^{3+}}\right) \tag{3b}$$

$$s_2 = \frac{1}{2}\left(2^{[6]}X_{\mathrm{Fe}^{3+}} - {}^{[4]}X_{\mathrm{Fe}^{3+}}\right). \tag{3c}$$

Sack and Ghiorso (1991a) tabulate the relationships between these compositional and ordering parameters for various end-member and binary spinels. See the spinel volume web tool (http://magmasource.caltech.edu/calculator/) described below for more general bounds that the composition of a spinel implies for the range of possible values of the order parameters. Note that Sack and Ghiorso (1991a, b) originally included an order parameter for Cr that was later abandoned and that they numbered the order parameters 1–4; their s_4 corresponds to our s_2. Although general dependence of volume on order state was considered, in practice only $MgAl_2O_4$-rich, $MgFe_2O_4$-rich, and $FeAl_2O_4$-rich compositions show order dependence of volumes at fixed composition.

Taking into account the site occupancy restrictions:

$$1 = {}^{[4]}X_{\mathrm{Fe}^{2+}} + {}^{[4]}X_{\mathrm{Mg}^{2+}} + {}^{[4]}X_{\mathrm{Al}^{3+}} + {}^{[4]}X_{\mathrm{Fe}^{3+}} \tag{4a}$$

$$1 = {}^{[6]}X_{\mathrm{Fe}^{2+}} + {}^{[6]}X_{\mathrm{Mg}^{2+}} + {}^{[6]}X_{\mathrm{Al}^{3+}} + {}^{[6]}X_{\mathrm{Fe}^{3+}} + {}^{[6]}X_{\mathrm{Ti}^{4+}} + {}^{[6]}X_{\mathrm{Cr}^{3+}}, \tag{4b}$$

expressions mapping mole fractions of cations into our chosen compositional and ordering variables may be readily derived.

The previously mentioned experiments of Doroshev et al. (1997), Brey et al. (1999), and Girnis et al. (2003) were quenched with an unknown ordering state. In order to use this data, we converted the reported oxide wt% into moles of cations. Note that the Fe^{2+}/Fe^{3+} ratio is calculated based on stoichiometry for this type of data, that is, the total anion charge is −8, so the total charge of the cations must equal +8. We assumed the experimental P and T conditions represented conditions corresponding to equilibrium ordering state, and applied the MELTS ordering model (Sack and Ghiorso 1991b). Once we recast the electron microprobe data into the site occupancy model, we are able to calculate Eqs. 2a–2e and proceed as above. Measurements not included in the calibration dataset but used for comparison (e.g., Golla-Schindler et al. 2005) were treated in a similar way; reported synthesis conditions or annealing temperatures were used if available and, where necessary, forward models were repeated for a range of plausible equilibrium temperatures.

Standard-state end-member properties included in our model are molar volume at reference pressure $P_o = 1$ bar and reference temperature $T_o = 298.15$ K (V^o), coefficient of thermal expansion (α), isothermal bulk modulus (K_{oT}), and the pressure derivative of the bulk modulus (K'). The general expression for the molar volume of a crystalline solid is $V = V_{\mathrm{ideal}} + V_{\mathrm{excess}}$, where excess volume of mixing is determined by an appropriate mixing model. The expression for V_{ideal} as a function of pressure, temperature, and composition is:

$$V_{\mathrm{ideal}} = \sum_i X_i V_i(P,T) \tag{5}$$

where $i = [\mathrm{sp}, \mathrm{ch}, \mathrm{uv}, \mathrm{mt}, \mathrm{hc}]$. V_i (P, T) is found by using Newton's method to search along the high-T Vinet equation of state,

$$P = 3K_{\mathrm{oT},i}\left(\frac{V_i}{V_i^{\mathrm{o}}}\right)^{-2/3}\left[1-\left(\frac{V_i}{V_i^{\mathrm{o}}}\right)^{1/3}\right] exp\left\{\frac{3}{2}\left(K_i'-1\right)\times\left[1-\left(\frac{V_i}{V_i^{\mathrm{o}}}\right)^{1/3}\right]\right\} + \alpha_i K_{\mathrm{oT},i}(T-T_{\mathrm{o}}). \tag{6}$$

The Vinet formalism is applied to each end-member composition at the P and T of interest, and the resulting volumes are mixed to construct the ideal term. Initial estimates of V^o, α, K_{oT}, and K' for each end member came from the provisional xMELTS spinel volume model (Ghiorso 2004b) except that K_{oT} values were taken from ultrasonic studies where available.

During model calibration, we considered excess volume terms of the symmetric regular solution form $W_{ij}X_iX_j$, asymmetric regular solution form $W_{ij}X_iX_j + \mathrm{d}W_{ij}X_iX_j$ $(X_i - X_j)$, and special terms dependent on ordering parameters. We allowed terms to depend on P and T as a way to encode non-ideal mixing of compressibility or thermal expansion without resorting to use of explicitly P- and T-dependent expressions for K_{oT}, K', or α.

Ultimately, however, we found that such *P*- and *T*-dependent parameters were not justified by the data.

Although it can be used in any context where a model of spinel molar volume is required, the present model is designed to be compatible with the activity-composition and ordering model of Sack and Ghiorso (1991a, b), which accounts for the standard state, exchange, reciprocal, and excess energies among the same set of independent and dependent end members adopted here and computes equilibrium site occupancy by Gibbs energy minimization. In formulating an extension to describe molar volumes, we begin of course by adopting the Sack and Ghiorso set of independent end members to define the standard-state contribution to the volume as a function of pressure and temperature. However, in modeling the excess and ordering volumes, we have a choice. We might adopt a parameter set strictly parallel to the parameters of the Sack and Ghiorso enthalpy model or we might formulate a new model guided by the volume data available. The former approach has some theoretical justification in that non-ideal enthalpy and volume of solutions both arise from the same microscopic effect, namely mismatch of ionic radii of substituting cations. However, the Sack and Ghiorso enthalpy model has 32 parameters, which turns out to be many more than are needed to describe the non-ideal component of volume behavior. The formulation of the enthalpy model may not yield a stable minimum set of parameters when fit to the volume data in a conservative way. In practice, the volume data set can be fit with a much smaller set of parameters with a minimum of parameter correlation if we choose a different formulation for excess volumes and volumes of ordering. Since our interest is in creating the most useful and reliable model for use in macroscopic thermodynamic applications, we have therefore adopted a new formulation for the non-ideal parts of our volume model, not parallel to the formulation of the enthalpy and ordering model, even though the result may provide less insight into the microscopic origin of the excess volumes.

Model calibration summary

A full description of the strategy for calibration, including parameters deemed significant or negligible and data used or excluded, is provided in the electronic appendix (Electronic Supplementary Material 3). In summary, the standard-state end-member properties, ordering terms, and contributions to selected symmetric regular solution terms were first calibrated to ambient, high-*T*, and high-*P* data for all end members, including the dependent end members $MgCr_2O_4$, $MgFe_2O_4$, and Mg_2TiO_4. The provisional regular solution terms accounted for the volume of reaction for the formation of the dependent end members by Fe–Mg exchange and were constructed in a way that was consistent with the data for binary and ternary spinels. Then, the remaining ambient pressure and temperature data were used to calibrate additional contributions to V_{excess} as a function of composition. Finally, the small number of high-*T* and high-*P* data for intermediate compositions were checked to see whether they required any revisions to the model, which they did not.

We have developed a calibration scheme that is able to directly query a MySQL database containing phase equilibrium, site occupancy, and volume data. The calibration scheme is written in MATLAB™ and uses the MATLAB-MySQL interface written by Robert Almgren (http://www.mathworks.com/matlabcentral/fileexchange/8663-mysql-database-connector). For the database, we adapted the schema from the Library of Experimental Phase Relations (LEPR) (Hirschmann et al. 2008) to incorporate the cell parameters and site occupancy data, with suitable metadata, and made a number of internal changes that reflect the different ways in which the two databases are updated and accessed. The MATLAB-generated MySQL queries allow us to test the effect of including or excluding a particular data source or type of experiment (e.g., heated in situ vs. annealed and quenched) with minimal effort and without the need for intermediate files.

Three terms describe the observed linear volume dependence on each of the cation-ordering variables s_0, s_1, and s_2 (Fig. 3). The adopted standard states for $MgAl_2O_4$ and $FeAl_2O_4$ are sufficiently close to normally ordered (e.g., $s_1 = 0.99998$ for $FeAl_2O_4$) that we assume them to be perfectly so. In order for the s_0-dependent term to vanish at Mg-free compositions, we used the form $(s_0 - 1)/2$, multiplied by X_{sp}, as this represents total Mg cations per formula unit. Likewise, we multiplied the s_1-dependent term by total Al, given by $2(X_{sp} + X_{hc})$. End-member Fe_3O_4 is approximated as perfectly inversely ordered and the s_2 term is multiplied by total Fe^{3+}, which is simply $2X_{mt}$ (see Eq. 7). The resulting ordering-composition cross-terms account for nearly all the excess volume along several key binaries: notably Fe_3O_4–Fe_2TiO_4 (Bosi et al. 2009) and $MgAl_2O_4$–$FeAl_2O_4$ (Andreozzi and Lucchesi 2002).

That no additional excess volume terms were required on the $MgAl_2O_4$–$FeAl_2O_4$ join was particularly fortuitous as it meant that the Cr^{3+}-, Fe^{3+}-, and Ti^{4+}-bearing spinel subsystems could be considered separately when choosing between candidate parameters. This process is described in more detail in the electronic appendix. Briefly, we chose the minimum number of parameters that could reasonably describe the ordering-adjusted volume surface for each reciprocal square (e.g., $MgAl_2O_4$–$MgCr_2O_4$–$FeCr_2O_4$–$FeAl_2O_4$) before moving our attention to other joins, such as Fe_3O_4–Fe_2TiO_4 and Fe_3O_4–$FeCr_2O_4$, and to multicomponent spinels.

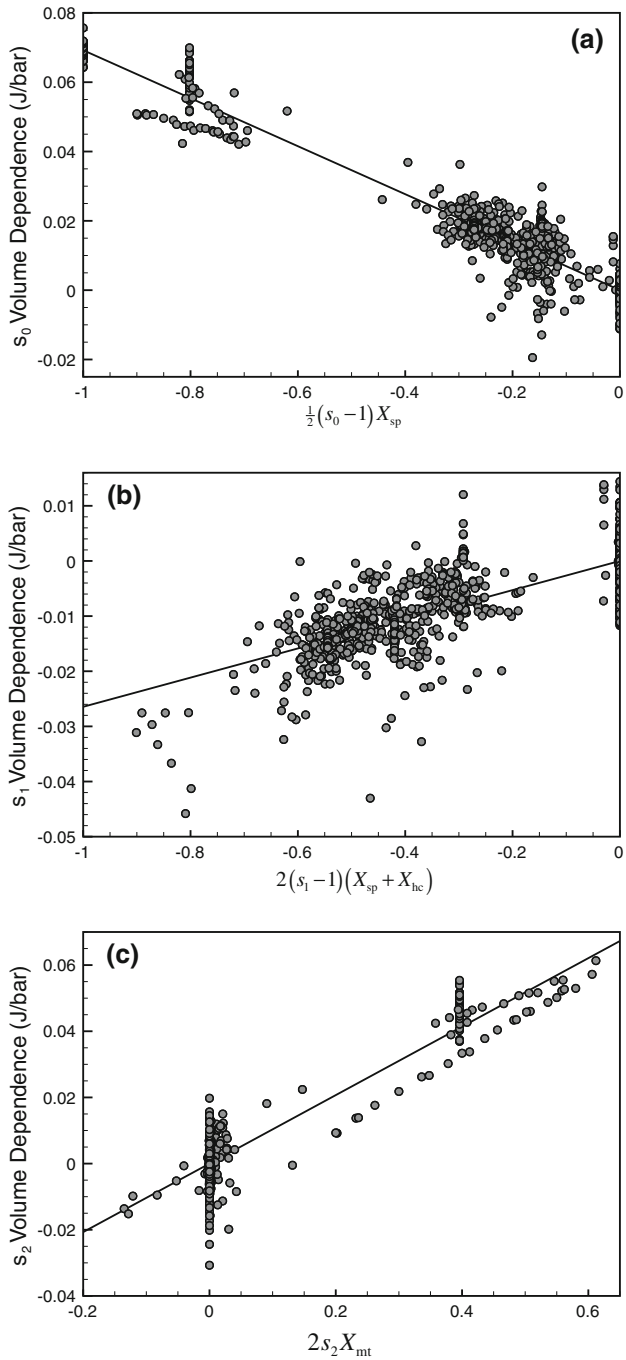

Fig. 3 Order dependence of observed volume versus ordering term for **a** s_0, **b** s_1, and **c** s_2. The order dependence for s_0, for example, is calculated by subtracting the model V_{ideal} and all other model terms not dependent on s_0 from the observed volume, V_{obs}. The linearity of the *data* shows the simple form of the order dependence of the data and the slope of the linear trend is proportional to the W_{s0} parameter (see Eq. 7). The corresponding calculations were done for s_1 and s_2. The *solid lines* are the model order dependences, plotted over the relevant range of ordering states

When calibrating the independent and dependent end-member data, we were careful not to activate excess volume terms along joins, such as $FeCr_2O_4$–$MgCr_2O_4$ (Lenaz et al. 2004), which showed little or no deviation from ideality once any ordering effects were subtracted. This strategy meant that certain combinations of solution parameters (e.g., $W_{mt\text{-}sp} - W_{mt\text{-}hc}$) were constrained by the end-member data. In the second stage calibration, end-member properties and ordering parameters were fixed; instead, we adjusted the existing excess volume terms (i.e., $W_{sp\text{-}ch}$, $W_{hc\text{-}ch}$, $W_{mt\text{-}sp}$, and $W_{mt\text{-}hc}$) and introduced two new terms ($dW_{sp\text{-}ch}$ and $W_{ch\text{-}mt}$) in a way that did not disturb the fit for the dependent end members.

We used the Bayesian information criterion (BIC) (Schwarz 1978), along with analysis of the reduced χ^2 statistic, to measure how efficiently our parameterized model predicts the data. Since we do not have information on measurement error for site occupancies, we are required to estimate the error in observed volume for calculating reduced χ^2. The BIC assigns a penalty term that is based on the complexity, or number of parameters, of the model. The formula is BIC $= -2\ \ln(L) + k\ \ln(n)$, where $\ln(L)$ is the optimized log-likelihood function associated with a particular model, k is the number of model parameters, and n is the number of observations associated with $\ln(L)$. By applying the BIC iteratively to the excess volume parameters and analyzing reduced χ^2, for example, all excess terms involving X_{uv} were found to be insignificant.

In all stages of the model, each of the five explicit end members has a pure component equation of state described by four parameters: V^o, α, K_{oT}, and K' (Tables 2, 3, 4). The additional parameters of the preferred final model include six excess terms along compositional binaries and three order-dependent terms. The values of the excess volume and order-dependent parameters are given in Table 5. The full expression of the model is:

$$\begin{aligned} V(X,T,P,s) = &\sum_i X_i V_i(T,P) \\ &+ W_{hc-ch}X_{hc}X_{ch} + W_{ch-mt}X_{ch}X_{mt} \\ &+ W_{sp-ch}X_{sp}X_{ch} + dW_{sp-ch}X_{sp}X_{ch}(X_{sp} - X_{ch}) \\ &+ W_{mt-hc}X_{mt}X_{hc} + W_{mt-sp}X_{mt}X_{sp} \\ &+ \frac{(s_0 - 1)}{2} W_{s0}X_{sp} + 2(s_1 - 1)W_{s1}(X_{sp} + X_{hc}) \\ &+ 2s_2 W_{s2}X_{mt}. \end{aligned} \quad (7)$$

This model fits virtually all of the data to within 0.02 J/bar/mol, or better than 0.5 % in volume (Figs. 4, 5), with a few exceptions for the studies of Antao et al. (2005a, b), Finger et al. (1986), Haavik et al. (2000), and Méducin et al. (2004) (see electronic appendix for exclusion criteria for these studies). The mean of the absolute values of the residuals for calibrated data is 0.0038 J/bar/mol and the root mean squared error is 0.0053 J/bar/mol. The goodness-of-fit of the model is displayed in Fig. 4, where observed molar volume is plotted first against the volume

Table 2 Optimized standard-state end-member molar volume for given ordering state

	V^o (J/bar/mol)	1σ[a]	Ordering state	[s_0, s_1, s_2]	a (Å)	ρ (kg m^{-3})
$MgAl_2O_4$	3.9722	1.7×10^{-4}	Normal	[1, 1, 0]	8.0808	3,582
$FeCr_2O_4$	4.4243	3.9×10^{-4}	Normal	[0, 0, 0]	8.3765	5,059
Fe_2TiO_4	4.6873	3.1×10^{-4}	Normal	[0, 0, 0]	8.5393	4,769
Fe_3O_4	4.4553	5.5×10^{-4}	Inverse	[0, 0, 0]	8.3960	5,197
$FeAl_2O_4$	4.0871	2.0×10^{-4}	Normal	[0, 1, 0]	8.1580	4,253

[a] Bootstrap estimation of s.d. for V^o, holding other parameters at optimal values

Table 3 Standard-state end-member coefficient of thermal expansion

	$\alpha(10^{-5})$ (K^{-1})	1σ[a]
$MgAl_2O_4$	2.4413	3.8×10^{-8}
$FeCr_2O_4$[b]	2.1691	–
Fe_2TiO_4	3.3458	4.3×10^{-8}
Fe_3O_4	3.3376	2.1×10^{-7}
$FeAl_2O_4$	2.6431	2.7×10^{-8}

[a] Bootstrap estimation of s.d. for α, holding other parameters at optimal values

[b] Value of α was held constant (see text)

Table 4 Bulk moduli and pressure derivatives of end members

	K_{oT} (GPa)	K'
$MgAl_2O_4$	190.8[a]	6.77[a]
$FeCr_2O_4$	203.3[b]	6.5[c]
Fe_2TiO_4	181[d]	5.5[d]
Fe_3O_4	181[e]	5.5[e]
$FeAl_2O_4$	210.3[f]	5.5[d]

[a] From Levy et al. (2003)

[b] From Doraiswami (1947)

[c] Constrained using data of Fan et al. (2008) (see appendix)

[d] Assumed to be equal to that of Fe_3O_4 (see text)

[e] From Nakagiri et al. (1986)

[f] From Wang and Simmons (1972)

model with asymmetric excess on the Fe_3O_4–Fe_2TiO_4 join used in current versions of MELTS (Fig. 4a), then against an ideal volume model using the refined end-member equation of state coefficients from Tables 2, 3, 4 (Fig. 4b), and finally against the model volume from the full form of Eq. 7 (Fig. 4c). When compared with the ideal model (Fig. 4b), data for dependent end members $MgCr_2O_4$ and $MgFe_2O_4$ show parallel trends with fixed offsets from the equiline that correspond to the quantities $2(W_{sp\text{-}ch} - W_{hc\text{-}ch})$ and $2(W_{mt\text{-}sp} - W_{mt\text{-}hc})$, respectively. The residuals in the final model are uncorrelated with observed molar volume and are nearly all $\leq$0.02 J/bar/mol for data accepted into the calibration set (Fig. 5). It is difficult to derive a more quantitative assessment of goodness-of-fit given uncertain knowledge of errors on composition, site occupancy, and molar volume in the calibration data.

Obtaining confidence bounds on the derived parameters is a separate issue from goodness-of-fit and can be addressed using bootstrap estimation (Efron 1982). Uncertainty bounds on each fitted parameter and a full correlation matrix for the parameter set derived from 50,000 bootstrap iterations are given in Electronic Supplementary Material 4 and 5. All parameters were varied, except those taken from ultrasonic studies or other sources (e.g., Levy et al.'s (2003) fit of K_{oT} and K' for $MgAl_2O_4$). The end-member properties are generally independent of one another; those trade-offs that exist are understandable given that the high-T properties of Fe^{3+}-, and Ti^{4+}-bearing spinels were constrained by data for the dependent end members $MgFe_2O_4$ and Mg_2TiO_4, respectively. Likewise, there is some correlation between V^o and ordering parameters for certain end members. As expected (see the electronic appendix), many of the purely compositional excess parameters are strongly correlated (e.g., $W_{sp\text{-}ch}$ with $W_{hc\text{-}ch}$, and $W_{mt\text{-}sp}$ with $W_{mt\text{-}hc}$) and are well-defined only in a joint sense. These observations emphasize that the calibrated parameters should only be used in the context of the full model derived here and that they may not be optimal descriptions of sub-systems if ideal and excess terms are separated. As noted above, the calibration data vary in coverage and quality and full estimates of measurement uncertainties are sparse, which means confidence bounds calculated using random sampling are probably unrealistically wide. Large uncertainties in the fit parameters do not necessarily feed into large uncertainties in the volumes calculated using the calibrated model, once the high degree of correlation between parameters is accounted for properly (Powell and Holland 1985). However, as the Vinet equation must be solved iteratively at each stage of the calculation in this case, such sophisticated propagation of uncertainties is neither straightforward nor likely to be that informative. Instead, for comparison, we obtained a more conservative confidence bound for each parameter, again using the bootstrapping technique but holding all other parameters at their optimal values; these uncertainties are reported in Tables 2, 3, and 5.

Table 5 Model parameters

		1σ[a]	
$W_{hc\text{-}ch}$	0.0108	0.018	(J/bar/mol)
$W_{ch\text{-}mt}$	0.0715	0.19	
$W_{sp\text{-}ch}$	0.0578	0.014	
$dW_{sp\text{-}ch}$	0.0489	0.063	
$W_{mt\text{-}hc}$	0.0833	0.025	
$W_{mt\text{-}sp}$	0.1020	0.025	
W_{s0}	-0.0692	0.00049	
W_{s1}	0.0264	0.00049	
W_{s2}	0.1035	0.0019	

[a] Bootstrap estimation of s.d. for each parameter, holding all other parameters at optimal values

A few aspects of the model remain underconstrained by data. There are neither ultrasonic velocities nor in situ high-*P* volume data for Ti-bearing compositions. We are forced to assume that the K_{oT} and K' for Fe_2TiO_4 are equal to those of Fe_3O_4 (Table 4). Given the low compressibility of spinels and the small Ti^{4+} concentrations in most spinels (and in particular in all the spinels that will be used for calibration of models of coexisting phases like garnet and pyroxene), this assumption is unlikely to have any significant effect on free energies within the pressure range of the spinel stability field. In addition, the value of α for $FeCr_2O_4$ was not varied during the calibration process. However, when the final model is used to calculate the effective α for a chromian spinel with composition $MgAl_{0.8}Cr_{1.2}O_4$, the value agrees with the one obtained from the lower temperature measurements (i.e., the ones made below the blocking temperature) of Levy and Artioli (1998, see Fig. 3a) to within 5.4×10^{-7} K^{-1}. In the absence of high-*T* structural refinements for $FeCr_2O_4$, we believe that the value of α adopted is the best estimate currently available.

Discussion

Model comparison

A comparison between our model and the model of Brey et al. (1999) is shown in Fig. 6. The gray surface in Fig. 6a shows the excess volume of the Brey et al. model in the $MgAl_2O_4$–$MgCr_2O_4$–$FeCr_2O_4$–$FeAl_2O_4$ reciprocal square, that is, the end-member contributions have been subtracted from the volume surface. The data plotted have also had the ideal end-member contributions to their volumes subtracted. The surface in Fig. 6b shows our proposed model in the same composition space as the Brey et al. model. Here, contributions from the end members and from our model ordering terms have been subtracted from model and

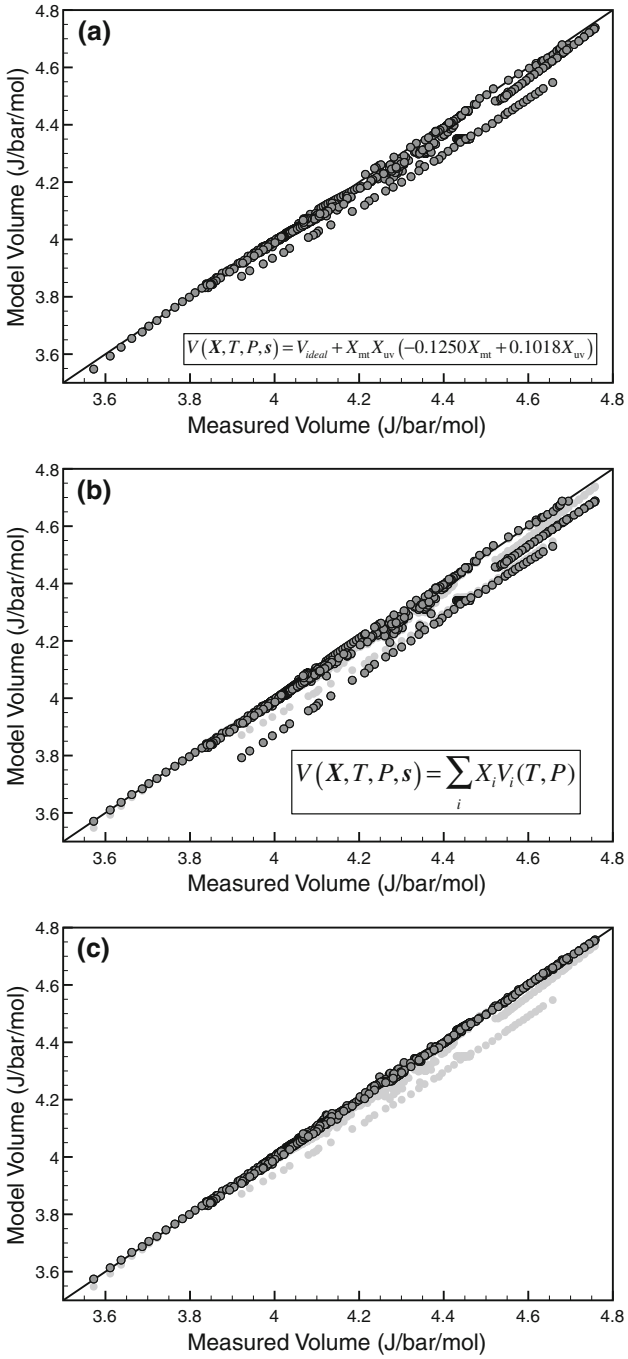

Fig. 4 Model volume versus measured volume. **a** Model results using spinel volume model currently implemented in MELTS (shown in *box*); **b** ideal model volume results after fitting of end members. Model results from **a** shown grayed out; **c** final model results. Model results from **a** shown grayed out

data. That the data appear smoother in Fig. 6b than in Fig. 6a shows that there is a distinct ordering effect on the volume that cannot be mapped into a purely compositional term (c.f. the Fe_3O_4–Fe_2TiO_4 join discussed below). Both models give similar fits to the data of Brey et al. and Doroshev et al. (1997) (diamonds), but the molar volume

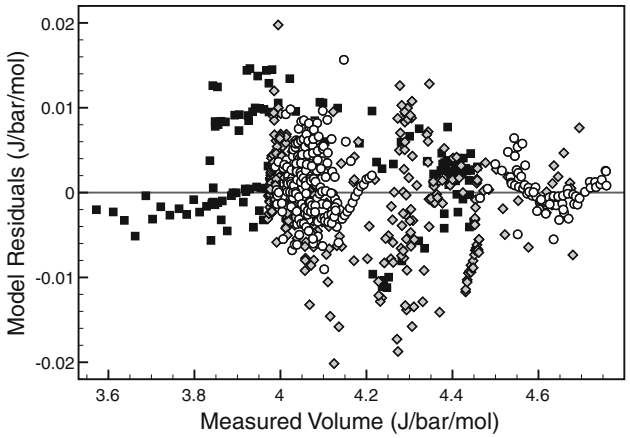

Fig. 5 Model residuals versus measured volume. *Gray diamonds* are samples measured at ambient-*P*, *T*, *open circles* are samples measured at high-*T* in situ, and *black squares* are samples measured at high-*P* in situ

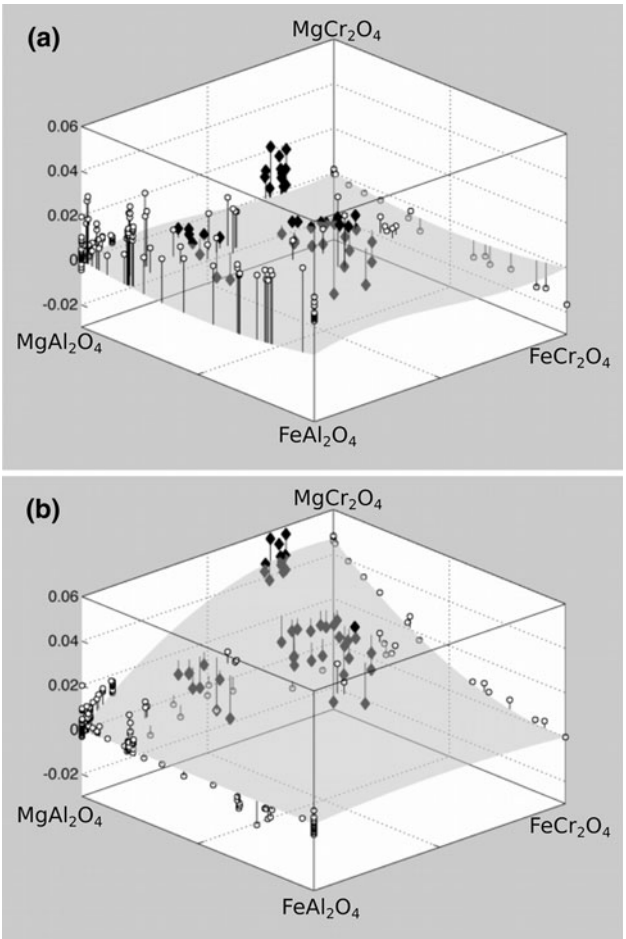

Fig. 6 Model volumes and data in the $MgAl_2O_4$–$MgCr_2O_4$–$FeCr_2O_4$–$FeAl_2O_4$ reciprocal square. End members are labeled at the corners. **a** *Gray surface* is the model of Brey et al. (1999) with end-member contributions subtracted. *Diamonds* are the data of Brey et al. (1999) and Doroshev et al. (1997); *open circles* are the rest of the room-*T*, *P* calibration dataset with <5 % magnetite or ulvöspinel component; **b** *Gray surface* is the model presented in this work, with end-member and ordering contributions subtracted. *Symbols* are the same as in (**a**)

of $FeCr_2O_4$ is more tightly constrained in our model due to the availability of data from Lenaz et al. (2004). Unlike Brey et al., we explicitly account for the dependent end member ($MgCr_2O_4$ in our model; $FeAl_2O_4$ in theirs) so our model predicts a warped volume surface. Finally, by making the asymmetrical excess volume term a function of X_{sp} and X_{ch}, rather than X_{Cr} and X_{Al}, our model is able to provide a much better fit to the rest of the data in the composition space (circles in Fig. 6).

The surface in Fig. 7a shows our model for spinels in $MgAl_2O_4$–$MgFe_2O_4$–Fe_3O_4–$FeAl_2O_4$ space; again, the end-member and ordering contributions have been subtracted from the model surface and the data. The model along the $MgAl_2O_4$–Fe_3O_4 binary is plotted in Fig. 7b, along with the model of Mattioli et al. (1987); the magnitudes of the positive, symmetric excess terms of the two models along this join are similar, and differences of up to $\sim$0.004 J/bar are due to different standard-state volumes for Fe_3O_4. The ordering state of Fe_3O_4 is particularly hard to quench, since it involves only electron exchange rather than cation mobility; hence, in Fig. 7b, we show curves with and without the modeled volume contribution due to ordering. A significant part of the asymmetry observed by Mattioli et al. on this join is apparently attributable to the composition-dependent closure temperature of the ordering reaction. Once these systematic differences in order state and measured volumes for compositions approaching pure Fe_3O_4 are accounted for, the data do not seem to justify an asymmetric excess volume term like the one used by Mattioli et al. The calibration data of Nakatsuka et al. (2004) ($MgAl_2O_4$–$MgFe_2O_4$) and the comparison data of Golla-Schindler et al. (2005) ($FeAl_2O_4$–Fe_3O_4) also support the simpler symmetric formalism (Fig. 7a).

The current spinel volume model formulation in MELTS and pMELTS includes asymmetric excess volume terms for the Fe_3O_4–Fe_2TiO_4 binary (Sack and Ghiorso 1991a), whereas in our model, the asymmetry comes solely from the ordering contribution to the volume (Fig. 8). The asymmetry in the volume variation is subtle, though well resolved by the data. The strong preference of Ti^{4+} for the octahedral site limits the configurational freedom along this join but the Mössbauer spectroscopic measurements of Bosi et al. (2009) indicate a sigmoidal variation in s_2 with X_{uv}. Deviations from the Akimoto (1954) ordering model (equivalent to setting $s_2 = 0$) have the same sense as the deviations from Vegard's Law, so it is not surprising that introducing an ordering dependence to the volume model may reduce the need for asymmetric interaction

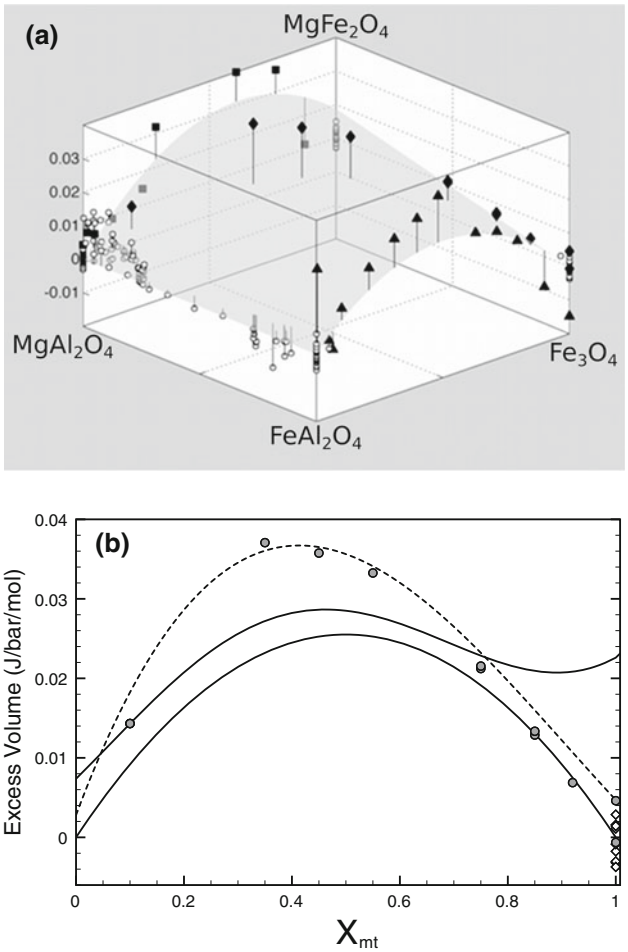

Fig. 7 **a** Excess model volume in the $MgAl_2O_4$–$MgFe_2O_4$–Fe_3O_4–$FeAl_2O_4$ reciprocal square. End members are labeled at the corners. *Gray* surface is the model presented in this work, with end-member and ordering contributions subtracted. *Open circles* are the room *T*, *P* calibration data with <5 % chromite or ulvöspinel component; *diamonds* are the data of Mattioli et al. (1987), only the most stoichiometric data (samples synthesized at 1,400 °C and oxygen fugacity of 10^{-4} atm) are plotted; *triangles* are the data of Golla-Schindler et al. (2005) for an equilibration temperature of 1,100 °C (varying this value within the stated range of annealing temperatures has little effect); *squares* are the data of Nakatsuka et al. (2004); data from Zhao et al. (1998) ($MgFe_2O_4$–Fe_3O_4) are not shown due to minor amounts of Ca in the analyses; **b** excess model volumes along the $MgAl_2O_4$–Fe_3O_4 binary. The *upper solid line* is the model excess volume along this join, including ordering states calculated with the MELTS ordering routine for Mattioli et al.'s experimental temperature of 1,400 °C. The *lower solid line* is the excess volume model plotted without additional ordering effects, that is, the order is perfectly normal at spinel and perfectly inverse at magnetite. The *dashed line* is the excess volume model of Mattioli et al. (1987); *gray circles* are the data of Mattioli et al. (1987); *open diamonds* are calibration data for the magnetite end member, measured at ambient conditions; the optimized end-member contributions from this work have been subtracted from models and data

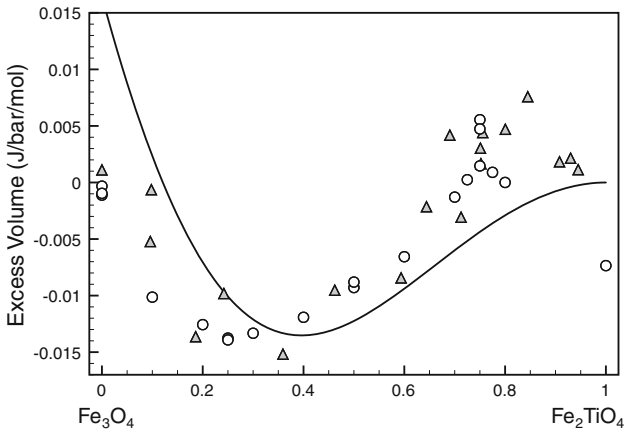

Fig. 8 Excess model volume (*black curve*) along the Fe_3O_4–Fe_2TiO_4 binary. The ordering state is calculated using the MELTS ordering routine at 1,100 °C; in other respects, the volume is calculated for ambient conditions. *Open circles* are the data of Wechsler et al. (1984) and *gray triangles* are the data of Bosi et al. (2009). Optimized end-member contributions from this work have been subtracted from the data. The volume along this binary is treated as ideal in the present model; asymmetry along this join is captured in the model by the effect of ordering alone

parameters. However, inasmuch as the ordering terms were calibrated only with data for pure $MgFe_2O_4$ (s_0 and s_2), $MgAl_2O_4$ (s_0 and s_1), and $FeAl_2O_4$ (s_1), the result that excess volume along the Fe_3O_4–Fe_2TiO_4 binary may be completely explained in this way is unexpected. Although we cannot properly constrain the nature of Ti^{4+} mixing in spinel, the notion that same-site substitution is nearly ideal for volume (i.e., excess volumes of mixing are due to ordering among the other cations) is supported by the few data available within the Ti-bearing subsystem.

The MELTS ordering model of Sack and Ghiorso (1991a, b) predicts a cation distribution that is independent of pressure because the accompanying volume model is ideal. As shown here, ordering effects can successfully explain all of the observed symmetric excess volumes of mixing on the $MgAl_2O_4$–$FeAl_2O_4$ join (Andreozzi and Lucchesi 2002), and the $MgAl_2O_4$–Mg_2TiO_4 and $FeAl_2O_4$–Fe_2TiO_4 binaries (Muan et al. 1972), as well as the aforementioned variation along Fe_3O_4–Fe_2TiO_4 (Bosi et al. 2009). The ordering parameters in our model also capture most of the mixing behavior along the Fe_3O_4–$FeCr_2O_4$ join (Robbins et al. 1971; Woodland et al. 2009) (Fig. 9). In our model, the excess volume term along this join is symmetric and constrained by data elsewhere in the composition space; introduction of the s_2 ordering term accounts for the asymmetry in the data (which were not included in the calibration). Furthermore, when the MELTS ordering model (Sack and Ghiorso 1991a, b) is updated to use our volume expression in the self-consistent calculation of ordering state by Gibbs energy minimization, it successfully predicts the high-*P*, *T* results of Antao et al. (2005b) for $MgFe_2O_4$ (Fig. 10). Note that the Antao et al. study was not included in the calibration dataset (see electronic

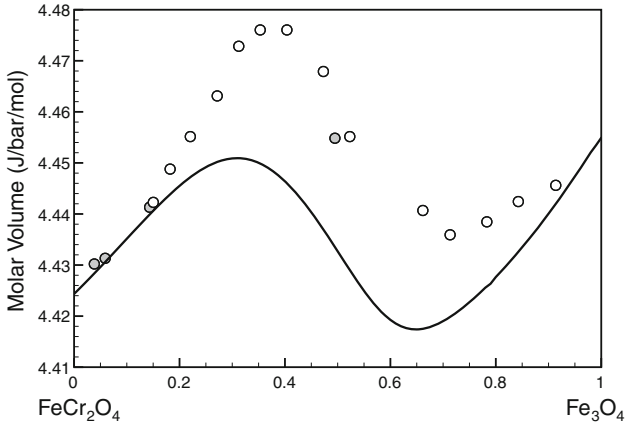

Fig. 9 Model volume (*black curve*) along the $FeCr_2O_4$–Fe_3O_4 binary, plotted with the data of Robbins et al. (1971) (*open circles*) and Woodland et al. (2009) (*gray circles*). The model curve is calculated using the MELTS ordering routine and the volume model from this work at ambient conditions. This binary is modeled with a symmetric excess term. The asymmetry of the data, which were not included in the calibration, is captured by the s_2 ordering term

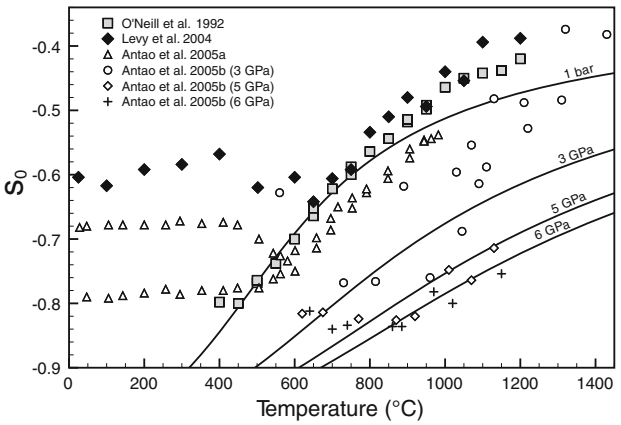

Fig. 10 Order variable s_0 versus temperature for pure $MgFe_2O_4$ data. The Levy et al. (2004) and Antao et al. (2005a, b) data were measured at high-*T*, in situ. O'Neill et al. (1992) samples were annealed over a range of temperatures; the annealing *T* is plotted here. The solid lines are calculated using the updated MELTS ordering model at 1 bar, 3GPa, 5GPa, and 6GPa for pure $MgFe_2O_4$

appendix) but the observed variation in volume with *P* and *T* is nevertheless consistent with the model presented here. The general role of order–disorder reactions in mineral volumes and compressibilities has been discussed by Hazen and Navrotsky (1996) and illustrated for the highly order-sensitive spinel $CoFe_2O_4$ by O'Neill and Navrotsky (1983). Spinel molar volume is a specific function of the tetrahedral (A–O) and octahedral (B–O) bond distances. The volume is about twice as sensitive to the B–O distance as it is to the A–O distance. Given differences in the ionic radii of cations in different coordination environments and valence states, it is therefore not surprising that spinel volumes are strongly order-dependent. Hazen and Navrotsky argue that such behavior is most pronounced when there are changes in ionic charge and coordination number, such that order–disorder reactions in minerals like olivine and orthopyroxene (mostly involving Fe^{2+} and Mg on crystallographically distinct octahedral sites) should show smaller effects than those documented here for spinel. The pyroxene model of Sack and Ghiorso (1994a) includes an ordering contribution to the volume.

Applications

Klemme (2004) presented experimental reversals for the garnet–spinel transition reaction $MgCr_2O_4 + 4\ MgSiO_3 = Mg_3Cr_2Si_3O_{12} + Mg_2SiO_4$. Klemme (2004) and Klemme et al. (2009) used the experimental brackets to extract enthalpy of formation and standard-state entropy for the garnet end member knorringite ($Mg_3Cr_2Si_3O_{12}$). Klemme's (2004) values were designed to be consistent with the thermodynamic dataset of Holland and Powell (1990), whereas Klemme et al. (2009) used a later version (Holland and Powell 1998). When Hamecher et al. (2009) repeated the exercise using the provisional xMELTS thermodynamic dataset (based on Berman 1988, but updated to use the Vinet equation of state), the recovered standard-state entropy of $Mg_3Cr_2Si_3O_{12}$ was significantly lower than the values given by Klemme and co-workers. We tested the effect of our newly calibrated spinel model and found only a small difference with the result from Hamecher et al. (2009). We also used the expressions and thermodynamic data of Holland and Powell (1990, 1998) and retrieved essentially the same values as Klemme et al. (2009). We could reproduce the results of Klemme (2004) but only if we used the volume parameters taken from Klemme et al. (2009) for both $Mg_3Cr_2Si_3O_{12}$ and $MgCr_2O_4$, instead of those from Irifune et al. (1982) and Robie et al. (1979) (see Table 3 in Klemme 2004). Hence, while the volume properties of $MgCr_2O_4$ spinel clearly influence the location of the spinel–garnet transition in the MgO-Cr_2O_3-SiO_2 system, a final volume model for Cr-bearing garnet is required in order to update the Hamecher et al. (2009) thermodynamic data for $Mg_3Cr_2Si_3O_{12}$.

In the meantime, we can gauge the effect that the new spinel volume model might have on MELTS calculations by extracting a typical lherzolite spinel composition from pMELTS and comparing its molar volume before and after recalibration. At 1,000 °C and 3 GPa, in the Workman and Hart (2005) depleted mantle composition, pMELTS predicts a spinel of composition $Fe^{2+}_{0.42}Mg_{0.60}Fe^{3+}_{0.20}Al_{0.38}Cr_{1.40}Ti_{0.01}O_4$. The molar volume of this spinel at the applied conditions, calculated with the spinel molar volume model built into all versions of MELTS to date, is

$V(\boldsymbol{X}, T, P, \boldsymbol{s}) = 4.3285$ J/bar/mol, whereas the model proposed in this work yields $V(\boldsymbol{X}, T, P, \boldsymbol{s}) = 4.3564$ J/bar/mol, a difference $\delta V_{sp} = +0.0279$ J/bar/mol. Although a full internally consistent recalibration of all aspects of the MELTS model is needed to see all the consequences of such a difference, the following simple calculation gives a preliminary sense of the magnitude of possible effects.

The difference in spinel molar volume corresponds to a difference in the model Gibbs free energy of spinel at elevated pressure and hence in the Gibbs free energy change of any reaction involving spinel. Keeping other quantities constant, the resulting displacement in pressure of an equilibrium boundary can be found by comparing the change in Gibbs energy of reaction to the volume change across the reaction. In this way, we can estimate, for example, what change in modeled pressure of the spinel–garnet transition will result when the current model is assimilated into MELTS. This is of some interest, because the match between experimental determinations of this boundary and MELTS calculations performed between 1995 and 2004 turned out to depend on an error in the implementation of the garnet solid solution model that was applied during model calibration (Berman and Koziol 1991). Since that error was fixed (Smith and Asimow 2005), the model is no longer self-consistent and the spinel–garnet lherzolite reaction has been calculated at a pressure as much as 0.8 GPa lower than experimental constraints (Hamecher et al. 2009).

For simplicity, consider the spinel–garnet lherzolite reaction in the simple MgO-Al_2O_3-SiO_2 (MAS) system: $MgAl_2O_4 + 2Mg_2Si_2O_6 = Mg_3Al_2Si_3O_{12} + Mg_2SiO_4$. At equilibrium, the Gibbs free energy of reaction (ΔG_{rxn}) is zero, and $\frac{\partial \Delta G_{rxn}}{\partial P}\big|_T = \Delta V_{rxn}$. We make the approximation:

$$\delta P_T \approx \frac{\delta \Delta G_{rxn}}{\Delta V_{rxn}} = -\frac{\delta G_{sp}}{\Delta V_{rxn}}, \tag{8}$$

where δ refers to the finite change between the two models, and $\delta \Delta G_{rxn} = -\delta G_{sp}$ since we are not changing the properties of the other reactants or products. We can estimate the difference between models in the Gibbs free energy of spinel by making the approximation:

$$\delta G_{sp} = \int_{P_o}^{P} \delta V_{sp} dP \approx \delta V_{sp}(P - P_o), \tag{9}$$

which, for $\delta V_{sp} = +0.0279$ J/bar/mol and $P = 3$ GPa, gives $\delta G_{sp} \sim 837$ J/mol. ΔV_{rxn} for the MAS reaction at 1,000 °C and 3 GPa is -0.8243 J/bar/mol (from the MELTS model, but substituting the new spinel model would make less than a 4 % difference in this number). Hence, the approximate displacement in the equilibrium pressure of the reaction between the two models is $\delta P_T \approx +1{,}015$ bars $= +0.1$ GPa. This difference is in the right direction to address the error in the current MELTS model, but is not enough to explain the entire discrepancy. Recovering a self-consistent model that matches experimental constraints on the pressure of the spinel–garnet lherzolite reaction will require a full recalibration of the garnet and pyroxene activity-composition models, with the best available molar volume models built into the calibration.

Web tool

There may be many applications of a molar volume model for spinel solid solutions beyond the MELTS-based calculations discussed herein. However, the formulation of the present model in terms of MELTS end members and ordering variables may be an impediment to its wide application. Hence, we have provided an online tool (http://magmasource.caltech.edu/calculator/) whereby users may input a spinel either as site occupancy data (that is, both composition and ordering state are measured) or as electron probe data with specified P and T (that is, composition is measured but ordering state is not) or as mole fractions of end members (including dependent ones) with P and T. The data are processed in the same manner as the calibration data herein and assigned to MELTS end members. If site occupancy is not given, the updated MELTS ordering model (i.e., based on Sack and Ghiorso (1991a, b) but with the volume model presented here) is used to estimate site occupancy by Gibbs energy minimization. Much like annealed samples within the calibration dataset, there is an option to specify one set of P–T conditions for the equilibrium ordering state (P_S, T_S) and another for calculation of the measureable volume (P_V, T_V). The web tool automatically converts between the various input options, such as wt% oxides and site occupancy, and displays the results. Finally, V_{ideal} (as a function of P_V and T_V), V_{excess} (calculated with site occupancy data, or with the MELTS ordering model using P_S and T_S), and V_{total} (i.e., $V_{ideal} + V_{excess}$) and, where appropriate, their derivatives with the relevant P and T are returned to the user.

Future prospects

Many of the assumptions made in our model were required due to the lack of published full structural refinements for certain regions of composition, temperature, and pressure space. There is a dearth of data available for the volume of Ti- and Cr-bearing spinels: we found only one in situ high-T study for Ti-bearing spinel, Mg_2TiO_4 (O'Neill et al. 2003), and not a single in situ high-P (at ambient or elevated-T) dataset. Likewise, the Martignago et al. (2003) in situ high-T study of three natural samples along the

$MgAl_2O_4$–$MgCr_2O_4$ binary is the only full refinement we currently have for Cr-bearing spinels measured at elevated conditions. As detailed in our discussion of Haavik et al. (2000), Méducin et al. (2004), and Antao et al. (2005a, b) (see the electronic appendix), there are some substantial disagreements in the literature even among compositions that have been more widely studied, for example, $MgAl_2O_4$ and Fe_3O_4, and some hints that the behavior of spinel at simultaneous high-*P*, *T* may be more complex than at high-*P* or high-*T* conditions alone. On the other hand, recent systematic measurements of the site occupancy and volume of binary spinels (Andreozzi and Lucchesi 2002; Bosi et al. 2009) allowed us to calibrate the effect of ordering on volume in a way not possible when the MELTS spinel model was originally developed (Sack and Ghiorso 1991a). It is our hope that with the current advances in X-ray and neutron diffraction methods, more high-quality data will become available for these spinel compositions, particularly at simultaneous very high-*P, T*, enabling us to improve upon our model assumptions in future calibrations.

Acknowledgments We wish to thank Peter Luffi for identifying the garnet solid solution error in the original MELTS code, Ashley Nagle for pointing out the anomalously low spinel–garnet transition pressures obtained when the corrected garnet model is used, and Aaron Wolf for helpful discussions regarding statistical analysis. Comments by Associate Editor Jon Blundy are greatly appreciated, as are the reviews of two anonymous reviewers. This work was supported by the National Science Foundation and the American Recovery and Reinvestment Act through award 0838244.

References

Akimoto S (1954) Thermo-magnetic study of ferromagnetic minerals contained in igneous rocks. J Geomagn Geoelectr 6:1–14

Andreozzi GB, Lucchesi S (2002) Intersite distribution of Fe^{2+} and Mg in the spinel (sensu stricto)-hercynite series by single-crystal X-ray diffraction. Am Mineral 87:1113

Andreozzi GB, Princivalle F (2002) Kinetics of cation ordering in synthetic $MgAl_2O_4$ spinel. Am Mineral 87:838–844

Andreozzi GB, Princivalle F, Skogby H, Della Giusta A (2000) Cation ordering and structural variations with temperature in $MgAl_2O_4$ spinel: an X-ray single-crystal study. Am Mineral 85:1164–1171

Andreozzi GB, Lucchesi S, Skogby H, Della Giusta A (2001) Compositional dependence of cation distribution in some synthetic $(Mg, Zn)(Al, Fe^{3+})_2O_4$ spinels. Eur J Mineral 13:391–402

Antao SM, Hassan I, Parise JB (2005a) Cation ordering in magnesioferrite, $MgFe_2O_4$, to 982 °C using in situ synchrotron X-ray powder diffraction. Am Mineral 90:219–228

Antao SM, Hassan I, Crichton WA, Parise JB (2005b) Effects of high pressure and high temperature on cation ordering in magnesioferrite, $MgFe_2O_4$, using in situ synchrotron X- ray powder diffraction up to 1430 K and 6 GPa. Am Mineral 90:1500–1505

Asimow PD, Dixon JE, Langmuir CH (2004) A hydrous melting and fractionation model for mid-ocean ridge basalts: application to the Mid-Atlantic Ridge near the Azores. Geochem Geophys Geosyst 5. doi:10.1029/2003GC000568

Barnes SJ, Roeder PL (2001) The range of spinel compositions in terrestrial mafic and ultramafic rocks. J Petrol 42:2279–2302

Berman RG (1988) Internally-consistent thermodynamic data for minerals in the system Na_2O-K_2O-CaO-MgO-FeO-Fe_2O_3-Al_2O_3-SiO_2-TiO_2-H_2O-CO_2. J Petrol 89:168–183

Berman RG, Koziol AM (1991) Ternary excess properties of grossular-pyrope-almandine garnet and their influence in geothermobarometry. Am Mineral 76:1223–1231

Bhagavantam S (1955) Elastic properties of single crystals and polycrystalline aggregates. Proc Math Sci 41:72–90

Bosi F, Hålenius U, Andreozzi GB, Skogby H, Lucchesi S (2007) Structural refinement and crystal chemistry of Mn-doped spinel: a case for tetrahedrally coordinated Mn^{3+} in an oxygen-based structure. Am Mineral 92:27–33

Bosi F, Hålenius U, Skogby H (2009) Crystal chemistry of the magnetite-ulvöspinel series. Am Mineral 94:181–189

Bragg W (1915) The structure of magnetite and the spinels. Nature 95:561

Brey GP, Doroshev AM, Girnis AV, Turkin AI (1999) Garnet-spinel-olivine-orthopyroxene equilibria in the FeO-MgO-Al_2O_3-SiO_2-Cr_2O_3 system: I. Composition and molar volumes of minerals. Eur J Mineral 11:599–617

Buddington AF, Lindsley DH (1964) Iron-titanium oxide minerals and synthetic equivalents. J Petrol 5:310–357

Callen HB, Harrison SE, Kriessman CJ (1956) Cation distributions in ferrospinels. Theoretical Phys Rev 103:851–856

Carbonin S, Russo U, Della Giusta A (1996) Cation distribution in some natural spinels from X-ray diffraction and Mössbauer spectroscopy. Mineral Mag 60:355–368

Carbonin S, Martignago F, Menegazzo G, Dal Negro A (2002) X-ray single-crystal study of spinels: in situ heating. Phys Chem Miner 29:503–514

Carraro A (2003) Crystal chemistry of Cr-spinels from a suite of spinel peridotite mantle xenoliths from the Predazzo Area (Dolomites, Northern Italy). Eur J Mineral 15:681–688

Connolly JAD (2009) The geodynamic equation of state: What and how. Geochem Geophys Geosys 10. doi:10.1029/2009GC002540

Della Giusta A, Carbonin S, Ottonello G (1996) Temperature-dependent disorder in a natural Mg-Al-Fe2 + -Fe3 + -spinel. Mineral Mag 60:603–616

Dick HJB, Bullen T (1984) Chromian spinel as a petrogenetic indicator in abyssal and alpine- type peridotites and spatially associated lavas. Contrib Mineral Petrol 86:54–76

Doraiswami MS (1947) Elastic constants of magnetite, pyrite and chromite. Proc Math Sci 25:413–416

Doroshev AM, Brey GP, Girnis AV, Turkin AI, Kogarko LN (1997) Pyrope-knorringite garnets in the Earth's mantle: experiments in the MgO-Al_2O_3-SiO_2-Cr_2O_3 system. Russ Geol Geophys 38:559–586

Downs RT, Hall-Wallace M (2003) The American Mineralogist crystal structure database. Am Mineral 88:247–250

Dunitz J, Orgel L (1957) Electronic properties of transition-metal oxides-II: cation distribution amongst octahedral and tetrahedral sites. J Phys Chem Solids 3:318–323

Efron B (1982) The jackknife, the bootstrap, and other resampling plans. Soc Ind Appl Math, Philadelphia

Fan D, Zhou W, Liu C, Liu Y, Jiang X, Wan F, Liu J, Li X, Xie H (2008) Thermal equation of state of natural chromium spinel up to 26.8 GPa and 628 K. J Mater Sci 43:5546–5550

Finger LW, Hazen RM, Hofmeister AM (1986) High-pressure crystal chemistry of spinel ($MgAl_2O_4$) and magnetite (Fe_3O_4): comparisons with silicate spinels. Phys Chem Miner 13:215–220

Fleet ME (1981) The structure of magnetite. Acta Crystallogr B37:917–920

Fleet ME (1984) The structure of magnetite: two annealed natural magnetites, $Fe_{3.005}O_4$ and $Fe_{2.96}Mg_{0.04}O_4$. Acta Crystallogr C40:1491–1493

Gatta G, Kantor I, Boffa Ballaran T, Dubrovinsky L, McCammon C (2007) Effect of non-hydrostatic conditions on the elastic behaviour of magnetite: an in situ single-crystal X-ray diffraction study. Phys Chem Miner 34:627–635

Ghiorso MS (1990) Thermodynamic properties of hematite-ilmenite-geikielite solid solutions. Contrib Mineral Petrol 104:645–667

Ghiorso MS (2004a) An equation of state for silicate melts. I. Formulation of a general model. Am J Sci 304:637–678

Ghiorso MS (2004b) An equation of state for silicate melts. III. Analysis of stoichiometric liquids at elevated pressure: shock compression data, molecular dynamics simulations, and mineral fusion curves. Am J Sci 304:752–810

Ghiorso MS (2004c) An equation of state for silicate melts. IV. Calibration of a multicomponent mixing model to 40 GPa. Am J Sci 304:811–838

Ghiorso MS, Evans BW (2008) Thermodynamics of rhombohedral oxide solid solutions and a revision of the Fe-Ti two-oxide geothermometer and oxygen- barometer. Am J Sci 308:957–1039

Ghiorso MS, Kress VC (2004) An equation of state for silicate melts. II. Calibration of volumetric properties at 10^5 Pa. Am J Sci 304:679–751

Ghiorso MS, Sack RO (1991) Fe-Ti oxide geothermometry: thermodynamic formulation and the estimation of intensive variables in silicic magmas. Contrib Mineral Petrol 108:485–510

Ghiorso MS, Sack RO (1995) Chemical mass transfer in magmatic processes IV. A revised and internally consistent thermodynamic model for the interpolation and extrapolation of liquid-solid equilibria in magmatic systems at elevated temperatures and pressures. Contrib Mineral Petrol 119:197–212

Ghiorso MS, Hirschmann MM, Reiners PW, Kress III VC (2002) The pMELTS: a revision of MELTS for improved calculation of phase relations and major element partitioning related to partial melting of the mantle to 3 GPa. Geochem Geophys Geosyst 3. doi:10.1029/2001GC000217

Ghiorso, MS, Hirschmann, MM, Grove, TL (2007) xMELTS: A thermodynamic model for the estimation of magmatic phase relations over the pressure range 0–30 GPa and at temperatures up to 2500 °C. Eos Trans Am Geophys Union 88(52), Fall Meet Suppl Abstr V31C-0608

Girnis A, Brey G, Doroshev A, Turkin A, Simon N (2003) The system MgO-Al2O3-Cr2O3 revisited: reanalysis of Doroshev et al'.s (1997) experiments and new experiments. Eur J Mineral 15:953–964

Golla-Schindler U, O'Neill HStC, Putnis A (2005) Direct observation of spinodal decomposition in the magnetite-hercynite system by susceptibility measurements and transmission electron microscopy. Am Mineral 90:1278–1283

Haavik C, Stølen S, Fjellvåg H, Hanfland M, Häusermann D (2000) Equation of state of magnetite and its high-pressure modification: thermodynamics of the Fe-O system at high pressure. Am Mineral 85:514–523

Haggerty S (1971) Compositional variations in lunar spinels. Nat Phys Sci 233:156–160

Hamecher EA, Antoshechkina PM, Ghiorso MS, Asimow PD (2009) Thermodynamic calibration of Cr-Al exchange equilibria for garnet and spinel. Eos Trans Am Geophys Union 90(52), Fall Meet Suppl Abstr V31D-2056

Harrison RJ, Redfern SAT, O'Neill HStC (1998) The temperature dependence of the cation distribution in synthetic hercynite ($FeAl_{\sim 2}O_{\sim 4}$) from in situ neutron structure refinements. Am Mineral 83:1092–1099

Hazen RM, Navrotsky A (1996) Effects of pressure on order-disorder reactions. Am Mineral 81:1021–1035

Hill RJ (1984) X-ray powder diffraction profile refinement of synthetic hercynite. Am Mineral 69:937–942

Hirschmann MM, Ghiorso MS, Davis FA, Gordon SM, Mukherjee S, Grove TL, Krawczynski M, Medard E, Till CB (2008) Library of experimental phase relations (LEPR): a database and web portal for experimental magmatic phase equilibria data. Geochem Geophys Geosyst 9. doi:10.1029/2007GC001894

Holland TJB, Powell R (1990) An enlarged and updated internally consistent thermodynamic dataset with uncertainties and correlations: the system K_2O–Na_2O–CaO–MgO–MnO–FeO–Fe_2O_3–Al_2O_3–TiO_2–SiO_2–C–H_2–O_2. J Metamorph Geol 8:89–124

Holland TJB, Powell R (1998) An internally consistent thermodynamic data set for phases of petrological interest. J Metamorph Geol 16:309–343

Holland TJB, Powell R (2011) An improved and extended internally consistent thermodynamic dataset for phases of petrological interest, involving a new equation of state for solids. J Metamorph Geol 29:333–383

Irifune T, Ohtani E, Kumazawa M (1982) Stability field of knorringite $Mg_3Cr_2Si_3O_{12}$ at high pressure and its implication to the occurrence of Cr-rich pyrope in the upper mantle. Phys Earth Planet Inter 27:263–272

Ishii M, Nakahira M, Yamanaka T (1972) Infrared absorption spectra and cation distributions in $(Mn, Fe)_3O_4$. Solid State Commun 11:209–212

Ishii M, Hiraishi J, Yamanaka T (1982) Structure and lattice vibrations of Mg-Al spinel solid solution. Phys Chem Miner 8:64–68

Kessel R, Beckett JR, Stolper EM (2003) Experimental determination of the activity of chromite in multicomponent spinels. Geochim Cosmochim Acta 67:3033–3044

Klemme S (2004) The influence of Cr on the garnet–spinel transition in the Earth's mantle: experiments in the system MgO–Cr_2O_3–SiO_2 and thermodynamic modelling. Lithos 77:639–646

Klemme S, Ivanic TJ, Connolly JAD, Harte B (2009) Thermodynamic modelling of Cr-bearing garnets with implications for diamond inclusions and peridotite xenoliths. Lithos 112:986–991

Larsson L, O'Neill HStC, Annersten H (1994) Crystal chemistry of synthetic hercynite ($FeAl_2O_4$) from XRD structural refinements and Mössbauer spectroscopy. Eur J Mineral 6:39–51

Lavina B, Koneva A, Della Giusta A (2003) Cation distribution and cooling rates of Cr- substituted Mg-Al spinel from the Olkhon metamorphic complex, Russia. Eur J Mineral 15:435–441

Lavina B, Princivalle F, Della Giusta A (2005) Controlled time-temperature oxidation reaction in a synthetic Mg-hercynite. Phys Chem Miner 32:83–88

Lavina B, Cesare B, Alvarez-Valero AM, Uchida H, Downs RT, Koneva A, Dera P (2009) Closure temperatures of intracrystalline ordering in anatectic and metamorphic hercynite, $Fe^{2+}Al_2O_4$. Am Mineral 94:657–665

Lenaz D, Princivalle F (2005) The crystal chemistry of detrital chromian spinel from the southeastern Alps and outer Dinarides: the discrimination of supplies from areas of similar tectonic setting? Can Mineral 43:1305–1314

Lenaz D, Skogby H, Princivalle F, Hålenius U (2004) Structural changes and valence states in the $MgCr_2O_4$-$FeCr_2O_4$ solid solution series. Phys Chem Miner 31:633–642

Lenaz D, Braidotti R, Princivalle F, Garuti G, Zaccarini F (2007) Crystal chemistry and structural refinement of chromites from different chromitite layers and xenoliths of the Bushveld Complex. Eur J Mineral 19:599–609

Lenaz D, Logvinova AM, Princivalle F, Sobolev NV (2009) Structural parameters of chromite included in diamond and kimberlites from Siberia: a new tool for discriminating ultramafic source. Am Mineral 94:1067–1070

Levy D, Artioli G (1998) Thermal expansion of chromites and zinc spinels. Mater Sci Forum 278–281:390–395

Levy D, Pavese A, Hanfland M (2003) Synthetic $MgAl_2O_4$ (spinel) at high-pressure conditions (0.0001–30 GPa): a synchrotron X-ray powder diffraction study. Am Mineral 88:93–98

Levy D, Diella V, Dapiaggi M, Sani A, Gemmi M, Pavese A (2004) Equation of state, structural behaviour and phase diagram of synthetic $MgFe_2O_4$, as a function of pressure and temperature. Phys Chem Miner 31:122–129

Lindsley DH (1965) Iron-titanium oxides. Carnegie Inst Year B 64:144–148

Lucchesi S, Amoriello M, Della Giusta A (1998) Crystal chemistry of spinels from xenoliths of the Alban Hills volcanic region. Eur J Mineral 10:473–482

Martignago F, Dal Negro A, Carbonin S (2003) How Cr^{3+} and Fe^{3+} affect Mg–Al order–disorder transformation at high temperature in natural spinels. Phys Chem Miner 30:401–408

Martignago F, Andreozzi G, Dal Negro A (2006) Thermodynamics and kinetics of cation ordering in natural and synthetic Mg(Al, Fe3+)2O4 spinels from in situ high-temperature X-ray diffraction. Am Mineral 91:306–312

Mattioli GS, Wood BJ, Carmichael ISE (1987) Ternary-spinel volumes in the system $MgAl_2O_4$–Fe_3O_4–$\gamma Fe_{8/3}O_4$: implications for the effect of P on intrinsic fo_2 measurements of mantle-xenolith spinels. Am Mineral 72:468–480

Méducin F, Redfern SAT, Le Godec Y, Stone HJ, Tucker MG, Dove MT, Marshall WG (2004) Study of cation order-disorder in $MgAl_2O_4$ spinel by in situ neutron diffraction up to 1600 K and 3.2 GPa. Am Mineral 89:981–986

Menegazzo G, Carbonin S (1998) Oxidation mechanisms in Al-Mg-Fe spinels. A second stage: α-Fe_2O_3 exsolution. Phys Chem Miner 25:541–547

Millard RL, Peterson RC, Hunter BK (1995) Study of the cubic to tetragonal transition in Mg_2TiO_4 and Zn_2TiO_4 spinels by ^{17}O MAS NMR and Rietveld refinement of X-ray diffraction data. Am Mineral 80:885–896

Muan A, Hauck J, Löfall T (1972) Equilibrium studies with a bearing on lunar rocks. In: Proceedings of the Third Lunar Science Conference (Suppl 3). Geochim Cosmochim Acta 1:185–196

Nakagiri N, Manghnani MH, Ming LC, Kimura S (1986) Crystal structure of magnetite under pressure. Phys Chem Miner 13:238–244

Nakatsuka A, Ueno H, Nakayama N, Mizota T, Maekawa H (2004) Single-crystal X-ray diffraction study of cation distribution in $MgAl_2O_4$–$MgFe_2O_4$ spinel solid solution. Phys Chem Miner 31:278–287

Nell J, Wood BJ (1989) Thermodynamic properties in a multicomponent solid solution involving cation disorder: Fe_3O_4–$MgFe_2O_4$–$FeAl_2O_4$–$MgAl_2O_4$ spinels. Am Mineral 74:1000–1015

Nestola F, Ballaran T, Balic-Zunic T, Princivalle F, Secco L, Dal Negro A (2007) Comparative compressibility and structural behavior of spinel $MgAl_2O_4$ at high pressures: the independency on the degree of cation order. Am Mineral 92:1838–1843

O'Neill HStC, Navrotsky A (1983) Simple spinels: crystallographic parameters, cation radii, lattice energies, and cation distribution. Am Mineral 68:181–194

O'Neill HStC, Navrotsky A (1984) Cations distributions and thermodynamic properties of binary spinel solid solutions. Am Mineral 69:733–753

Oka Y, Steinke P, Chatterjee ND (1984) Thermodynamic mixing properties of Mg(Al, Cr)2O4 spinel crystalline solution at high temperatures and pressures. Contrib Mineral Petrol 87:196–204

O'Neill HStC, Dollase WA (1994) Crystal structures and cation distributions in simple spinels from powder XRD structural refinements: MgCr2O4, ZnCr2O4, Fe3O4, and the temperature dependence of the cation distribution in ZnAl2O4. Phys Chem Miner 20:541–555

O'Neill HStC, Annersten H, Virgo D (1992) The temperature dependence of the cation distribution in magnesioferrite (MgFe2O4) from powder XRD structural refinements and Mössbauer spectroscopy. Am Mineral 77:725–740

O'Neill HStC, Redfern S, Kesson S, Short S (2003) An in situ neutron diffraction study of cation disordering in synthetic qandilite Mg2TiO4 at high temperatures. Am Mineral 88:860–865

Pascal ML, Fonteilles M, Boudouma O, Principe C (2011) Qandilite from Vesuvius skarn ejecta: conditions of formation and miscibility gap in the ternary spinel—qandilite—magnesioferrite. Can Mineral 49:459–485

Passerini L (1930) Richerche sugli spinelli. II. I composti. $CuAl_2O_4$, $MgAl_2O_4$, $MgFe_2O_4$, $ZnAl_2O_4$, $ZnCr_2O_4$, $ZnFe_2O_4$, $MnFe_2O_4$. Gazz Chim Ital 60:389–399

Peterson RC, Lager GA, Hitterman RL (1991) A time-of-flight neutron powder diffraction study of $MgAl_2O_4$ at temperatures up to 1273 K. Am Mineral 76:1455–1458

Powell R, Holland TJB (1985) An internally consistent thermodynamic dataset with uncertainties and correlations: 1. Methods and a worked example. J Metamorph Geol 3:327–342

Powell R, Holland TJB, Worley B (1998) Calculating phase diagrams involving solid solutions via non-linear equations, with examples using THERMOCALC. J Metamorph Geol 16:577–588

Princivalle F, Della Giusta A, De Min A, Piccirillo E (1999) Crystal chemistry and significance of cation ordering in Mg-Al rich spinels from high-grade hornfels (Predazzo-Monzoni, NE Italy). Mineral Mag 63:257–262

Princivalle F, Martignago F, Del Negro A (2006) Kinetics of cation ordering in natural Mg(Al, Cr3+)2O4 spinels. Am Mineral 91:313–318

Redfern SAT, Harrison RJ, O'Neill HStC, Wood DRR (1999) Thermodynamics and kinetics of cation ordering in $MgAl_2O_4$ spinel up to 1600 °C from in situ neutron diffraction. Am Mineral 84:299–310

Reichmann HJ, Jacobsen SD (2004) High-pressure elasticity of a natural magnetite crystal. Am Mineral 89:1061–1066

Robbins M, Wertheim GK, Sherwood RC, Buchanan DNE (1971) Magnetic properties and site distributions in the system $FeCr_2O_4$–Fe_3O_4 ($Fe^{2+}Cr_{2-x}Fe_x^{3+}O_4$). J Phys Chem Solids 32:717–729

Robie RA, Hemingway BS, Fisher JR (1979) Thermodynamic properties of minerals and related substances at 298.15 K and 1 bar (1e5 Pa) pressures and at higher temperatures. US Geol Surv Bull 1452:1–456

Sack RO (1982) Spinels as petrogenetic indicators: activity-composition relations at low pressures. Contrib Mineral Petrol 79: 169–186

Sack RO, Ghiorso MS (1991a) An internally consistent model for the thermodynamic properties of Fe-Mg-titanomagnetite-aluminate spinels. Contrib Mineral Petrol 106:474–505

Sack RO, Ghiorso MS (1991b) Chromian spinels as petrogenetic indicators: thermodynamics and petrological applications. Am Mineral 76:827–847

Sack RO, Ghiorso MS (1994a) Thermodynamics of multi component pyroxenes: iI. Phase relations in the quadrilateral. Contrib Mineral Petrol 116:287–300

Sack RO, Ghiorso MS (1994b) Thermodynamics of multicomponent pyroxenes: III. Calibration of $Fe^{2+}(Mg)_{-1}$, $TiAl_2(MgSi_2)_{-1}$, $TiFe_2^{3+}(MgSi_2)_{-1}$, $AlFe^{3+}(MgSi)_{-1}$, $NaAl(CaMg)_{-1}$, $Al_2(MgSi)_{-1}$ and $Ca(Mg)_{-1}$ exchange reactions between pyroxenes and silicate melts. Contrib Mineral Petrol 118:271–296

Schwarz G (1978) Estimating the dimension of a model. Ann Stat 6:461–464

Sedler IK, Feenstra A, Peters T (1994) An X-ray powder diffraction study of synthetic (Fe, Mn)2TiO4 spinel. Eur J Mineral 6:873–885

Smith PM, Asimow PD (2005) Adiabat_1ph: a new public front-end to the MELTS, pMELTS, and pHMELTS models. Geochem Geophys Geosyst 6. doi:10.1029/2004GC000816

Stout M, Bayliss P (1980) Crystal structure of two ferrian ulvöspinels from British Columbia. Can Mineral 18:339–341

Taberna PL, Mitra S, Poizot P, Simon P, Tarascon J-M (2006) High rate capabilities Fe_3O_4- based Cu nano-architectured electrodes for lithium-ion battery applications. Nat Mater 5:567–573

Tabira Y, Withers RL (1999) Cation ordering in $NiAl_2O_4$ spinel by a 111 systematic row CBED technique. Phys Chem Miner 27:112–118

Verwey E, Heilmann E (1947) Physical properties and cation arrangement of oxides with spinel structures I. Cation arrangement in spinels. J Chem Phys 15:174–180

Waerenborgh JC, Figueiredo MO, Cabral JMP, Pereira LCJ (1994) Powder XRD structure refinements and ^{57}Fe Mössbauer effect study of synthetic $Zn_{1-x}Fe_xAl_2O_4$ ($0 < x \leq 1$) spinels annealed at different temperatures. Phys Chem Miner 21:460–468

Wang H, Simmons G (1972) Elasticity of some mantle crystal structures 1. Pleonaste and hercynite spinel. J Geophys Res 77:4379–4392

Wechsler BA, Von Dreele RB (1989) Structure refinements of Mg_2TiO_4, $MgTiO_3$ and $MgTi_2O_5$ by time-of-flight neutron powder diffraction. Acta Crystallogr B45:542–549

Wechsler BA, Lindsley D, Prewitt C (1984) Crystal structure and cation distribution in titanomagnetites ($Fe_{3-x}Ti_xO_4$). Am Mineral 69:754–770

Woodland AB, Bauer M, Ballaran TB, Hanrahan M (2009) Crystal chemistry of $Fe_3^{2+}Cr_2Si_3O_{12}$ – $Fe_3^{2+}Fe_2^{3+}Si_3O_{12}$ garnet solid solutions and related spinels. Am Mineral 94:359–366

Workman RK, Hart SR (2005) Major and trace element composition of the depleted MORB mantle (DMM). Earth Planet Sci Lett 231:53–72

Yamanaka T, Shimazu H, Ota K (2001) Electric conductivity of Fe_2SiO_4–Fe_3O_4 spinel solid solutions. Phys Chem Miner 28:110–118

Yang Z, Xia G-G, Li X-H, Stevenson JW (2007) (Mn, Co)3O4 spinel coatings on ferritic stainless steels for SOFC interconnect applications. Int J Hydrogen Energy 32:3648–3654

Zhao Y, Zhang Y, Bi C, Guo L (1998) The discovery of magnesioferrite from Au(Fe, Cu) magnesian skarn deposits and study of the magnesioferrite-magnesiomagnetite series. Acta Geol Sin 74:382–391